Hindawi
Journal of Nanomaterials
Volume 2024, Article ID 2970861, 30 pages
https://doi.org/10.1155/2024/2970861

Research Article

Colloid Systems and Interfaces Stability of Cerium Oxide Nanoparticles in Aqueous Environments: Effects of pH, Ionic Composition, and Suwanee River Humic and Fulvic Acids

Linlin Mu,[1] Mahsa Ghorbani,[1] Philippe C. Baveye,[2] and Christophe J. G. Darnault[1]

[1]*Department of Environmental Engineering and Earth Sciences, School of Civil and Environmental Engineering and Earth Sciences, Clemson University, 342 Computer Court, Anderson, SC 29625, USA*
[2]*Saint Loup Research Institute, 7 rue des Chênes, Saint Loup Lamairé 79600, France*

Correspondence should be addressed to Christophe J. G. Darnault; cdarnau@clemson.edu

Received 27 May 2023; Revised 21 December 2023; Accepted 27 December 2023; Published 29 January 2024

Academic Editor: Abdelwahab Omri

This study investigates the colloid systems and interfaces stability of cerium oxide nanoparticles in aqueous environments as a function of pH, monovalent cations (Na^+) and divalent cations (Ca^{2+}), and humic substances (humic acid (HA) and fulvic acid (FA)). Results show that the solution chemistry affected the colloidal stability and aggregation kinetics of CeO_2 NPs. The pH point of zero charge (pH_{PZC}) of CeO_2 NPs was measured at pH 10.2 with diameter of CeO_2 NPs aggregates of ~1,700 nm. The effects of Na^+ and Ca^{2+} and HA and FA on the magnitudes and rates of aggregation were pH-dependent. In addition, when salts were present in the aqueous systems, although the CeO_2 NPs were stable at $pH < pH_{PZC}$ (expect for 1 mM of $NaCl/CaCl_2$) and $pH > pH_{PZC}$ (except for 0.5 mM $CaCl_2$), the aggregation was enhanced at $pH = pH_{PZC}$, with the diameter of CeO_2 NPs in the ~1,300–3,600 nm range. HA also stabilized CeO_2 NPs under $pH > pH_{PZC}$ with an enhanced aggregation of $pH = pH_{PZC}$ with the diameter of CeO_2 NPs in the ~1,500–1,900 nm range, and in the presence of 0 and 1 mM of $NaCl/CaCl_2$ at $pH < pH_{PZC}$. At three pH levels (8.2, 10.2, and 12.2) and under all different electrolyte concentrations (0–1 mM of NaCl or $CaCl_2$), FA (0.14 mg/L) exhibited a greater degree of efficiency in stabilizing CeO_2 NPs than HA (5 mg/L), with CeO_2 NPs aggregates growing at low rates and resulting in diameter of ~95–115 nm.

1. Introduction

Revolutionary advances in the field of nanoscience and nanotechnology have played a key role in the development of new materials and technologies for products and applications to all the sectors of industry—agriculture, manufacturing, and services—and have impacted our daily life. Among the nanoparticles engineered in nanoscience, the metal nanoparticles (NPs) CeO_2 NPs are a common nanomaterial used increasingly in products and applications [1, 2]. CeO_2 NPs have unique physicochemical properties, such as strong ultraviolet (UV) radiation absorbing capacity, high capacity for donating and storing oxygen, and low Ce^{IV}/Ce^{III} redox potential [3–6]. CeO_2 NPs are used in exhaust gas catalysts in diesel fuel additives [7–9], capacitors and semiconductors in electronic devices [10, 11], antioxidants in medical products [12], UV-blocking agents in sunscreen [7], and polishing agents in manufacturing glass [8].

With the increasing use in products and applications, the presence of CeO_2 NPs in environmental components, such as soil, sediments, water, air, and biota, is inevitable. Although CeO_2 NPs in diesel fuel additives increase the efficiency of trapping particulate matter and decrease NO_x emissions during combustion in engines, CeO_2 NPs are present in the exhaust emissions that discharge into the air [7, 13, 14]. CeO_2 NPs released from fertilizers can also contaminate the soil. The estimated CeO_2 NPs concentrations in biosolids, which are calculated by using 2010's market study production estimates in three metropolitan areas (New York, Shanghai, and London), range from 0.53 to 9.1 mg/kg [15, 16]. By using the same method of estimation, the range of the concentration of CeO_2 NPs released from wastewater treatment plants into

waterbodies is 0.003–1.17 μg/L [15, 16]. Other possible sources of release of CeO_2 NPs into soil and water systems include discarded electronics or residue from coatings or sunscreen products [1, 17]. Once released into the environment, CeO_2 NPs may be contaminant carriers or serve as ecological and public health threats themselves.

The toxicity effects of CeO_2 NPs on plants, such as lettuce, rice, cucumber, tomato, and soybean, have been investigated [18–26]. For example, although the addition of CeO_2 NPs to fertilizer may enhance root growth in rice seedlings [27], it can alter the composition and nutritional values of crop plants, such as soybeans, cowpeas, corn, and mungbean [27–30]. Some studies have also involved determining the toxicity of CeO_2 NPs on microorganisms. Microbial communities were found to be inhibited by CeO_2 NPs during the wastewater treatment process [12]. The activities of soil enzymes in a soil–plant system were also affected by CeO_2 [31]. CeO_2 NP toxicity to invertebrates on land and in water systems has also been reported in studies involving earthworms, nematodes, algae, and phytoplankton [15, 32–34].

The transport of CeO_2 NPs in natural porous media (e.g., soil and aquifer systems) and in engineered porous media (e.g., sand filtration systems) was also the subject of study [35–40]. In terms of the physicochemical parameters, CeO_2 NP transport in saturated sand-packed columns was hindered in the presence of NaCl with high ionic strength (IS) values (larger than 10 mM) at pH 3 [37]. Organic matter enhanced the stability and mobility of CeO_2 NPs in the presence of 1 mM NaCl at pH 6.5 [41]. The increase of HA concentration from 0 to 10 mg/L or the decrease of IS from 100 to 1 mM markedly facilitated the transport of CeO_2 NPs more than the influence of the increase of pH from pH 7 to 10 [38]. The retention of CeO_2 NPs was observed in loamy sand as well as under high concentration levels of $CaCl_2$ and $MgCl_2$ at pH 8 [39].

Colloidal stability and aggregation state of engineered nanoparticles—such as CeO_2 NPs—are key criteria governing the environmental behavior of nanoparticles [42, 43]. The stability of nanoparticles controls their fate and transport in terrestrial and aquatic systems, bioavailability, and toxicity, as the size of the nanoparticles/nanoaggregates is essential in determining their reactivity [44, 45]. The stability of CeO_2 NPs is a function of their size [46–48], surface chemistry and capping agent [47, 49, 50], and surface charge [51, 52] which is influenced by the physicochemical conditions of the soil water environment the nanoparticles encounter, such as pH [45, 48, 53–56], IS [43, 53, 56–58], electrolyte types [48, 52, 56, 59, 60], and organic compounds [47, 52–54, 61, 62], including humic acid (HA) [43, 57, 63] and fulvic acid (FA) [45, 58, 63, 64].

In terms of various environmental parameters, one of the most importance of which was pH, the colloidal stability and aggregation of engineered nanoparticles were the subject of a number of studies [65–67]. The pH of suspensions affects the surface ionization of nanoparticles. The stability of NPs has been investigated in different electrostatic scenarios related to pH_{PZC}, specifically $pH > pH_{PZC}$, $pH = pH_{PZC}$, and $pH < pH_{PZC}$ [45, 68, 69]. For example, the pH_{PZC} of the uncoated CeO_2 NPs, which had a primary particle diameter 28 ± 10 nm and a specific surface area $27.2 \pm 0.9\ m^2/g$, is equal to 6.8 ± 0.1 [45]. An increase of the pH from 3 to 10 decreased the zeta potential from positive to negative values. Further, the size of the CeO_2 NP nanoaggregates was lower than 200 nm at $pH < pH_{PZC}$ and reached 800–1,500 nm at $pH = pH_{PZC}$.

IS plays an important role in controlling the behavior of NP stability [70–76]. The increase of IS, affecting NPs by electric double layer (EDL) compression, zeta potential reduction, and charge reversal by counterions, generally enhances NP aggregation [17, 77, 78]. Electrolyte valence is also an additional and important factor for determining the aggregation efficiency of electrolytes. For example, at pH 4.8 and 0.0128 M, $CaCl_2$ had a faster rate of aggregate formation of TiO_2 NPs than that of NaCl [79]. Other research also demonstrated that a lower critical coagulation concentration (CCC) was observed in CeO_2 NPs for Ca^{2+} (16 mM) than Na^+ (80 mM) with a proportionality fraction of $\varkappa^{-2.3}$ where $\varkappa$ is the counterion valence [52].

Natural organic matter (NOM), which contains humic substances (HS), polysaccharides, algal, and bacterial residues, also affects the stability of NPs [45, 80]. As a major component of NOM, HS is present in soil, water, and geological organic deposits. HS in natural water systems, which compose 20%–50% of NOM in the aquatic environment, have three components: HAs, FAs, and humin [45, 81]. HS functional groups, such as carboxylate, phenolate, amino, and thiol, can attach themselves to minerals or metal oxide bulk particles and NPs [82, 83]. NPs stability is affected by the NOM coating formation types on NP surfaces [84]. In addition, the concentration, composition, molecular mass, hydrophobicity, and polarity of NOM and the couple effects of NOM and pH, or different types of cations, also determine NP stability [85–87]. For instance, the stability of CeO_2 NPs and complexes of FA and CeO_2 NPs were studied at three pH levels (3, 7, 10) that corresponded to the positive ($pH < pH_{PZC}$), neutral ($pH = pH_{PZC}$), and negative ($pH > pH_{PZC}$) surface charge of CeO_2 NPs, respectively [45]. The environmental amount of FA (2 mg/L) at pH 3 ($pH < pH_{PZC}$) was capable of stabilizing CeO_2 NPs. The CCC of CeO_2 NPs for KCl shifted to higher levels (>500 mM) as the SRHA concentration increased (from 0 to 10 mg/L) at pH 5.7 [47]. At pH 5.7 and at a low SRHA concentration (1 mg/L), SRHA stabilized the CeO_2 NPs at a high KCl concentration (500 mM) [47].

Despite significant advances in the understanding of the mechanisms and parameters that govern the fate and behavior of engineered nanomaterials (ENMs) in the environment, "many knowledge gaps remain" [42]. Studying ENMs in "more complex real-world systems" and "relevant environmental systems" [42], as in aquatic systems, is essential to further the understanding of the fate and transport of ENMs in the earth's system of natural resources and to formulate regulations on their discharge in the aquatic, terrestrial, and atmospheric systems [42, 43].

Therefore, it is critical to further the understanding of the fate and behavior of prominent ENMs, like CeO_2 NPs, in complex environmental systems for the purpose of protecting

the ecosystems and human health [42, 43]. Most of all, knowledge of the "aggregation state" and "characterization of homo- and heteroaggregates" of ENMs in aquatic and terrestrial systems needs to be improved, as outlined by Surette et al. [42] in their assessment of research needs in the field of ENMs and their interactions with the environment. Moreover, Surette et al. [42] highlighted the need to explore the effects of specific physicochemical parameters of aqueous systems on ENMs. These parameters include "IS/composition, pH, and organic matter" and relate to research needs focusing on "experimental condition" as proposed by Surette et al. [42]. It also responds to the necessity to conduct studies exploring the fate of ENMs in aquatic systems as mentioned by Bathi et al. [43].

Understanding of the synergistic effect of the physical and chemical properties of CeO_2 NPs and the chemistry of their environment—pH, ionic composition, and NOM (HA and FA)—is essential to further the understanding of the processes governing the colloidal stability, interfacial interactions, and aggregation of CeO_2 NPs in water and environmental systems. Interfacial interactions govern the behavior of CeO_2 NPs in the environment, and their threat to public health and the environment. Yet, the synergy between CeO_2 NPs as a function of pH, ionic composition, and organic matter that induces alterations in colloid systems and interfaces stability is complex and varied. Then, it is crucial to investigate the self-interactions between CeO_2 NPs, the interactions between CeO_2 NPs and monovalent/divalent cations, and the interactions between CeO_2 NPs and monovalent/divalent cations-humic substance systems under different pH conditions, as well as their ensuing assemblage of structures/aggregation in order to discover their affect on the colloidal phenomena and interfacial interactions of CeO_2 NPs in aqueous environments.

As discussed in our recent study titled "Colloidal phenomena and aggregation mechanisms of cerium oxide nanoparticles in aqueous systems: Effects of monovalent and divalent cations, and Suwanee River humic and fulvic acids," colloid systems and interfaces stability of CeO_2 NPs in aqueous systems are impacted by electrolytes and organic matter [88]. Therefore, the objectives of this study are to (1) analyze the colloidal phenomena and interfacial interactions of CeO_2 NPs as a function of pH and determine the pH_{PZC}, (2) investigate the colloidal phenomena and interfacial interactions of CeO_2 NPs at three different pH regimes which relate to pH_{PZC} (below, at, and above pH_{PZC}) along with monovalent and metallic cation Na^+ or divalent and metallic cation Ca^{2+}, and (3) study the colloidal phenomena and interfacial interactions of CeO_2 NPs at three different pH regimes which relate to pH_{PZC} (below, at, and above pH_{PZC}) along with metallic cations (Na+ or Ca^{2+})—HS (HA or FA). A laboratory-scale batch experiment approach was conducted to assess and quantify the influence of pH, metal cations, IS, HA, and FA on the colloidal phenomena and interfacial interactions of CeO_2 NPs. Measurement techniques of dynamic light scattering (DLS) and electrophoretic light scattering (ELS) were utilized to determine the hydrodynamic diameter and zeta potential of CeO_2 NPs, respectively. Aggregation kinetics and attachment efficiency were calculated from the laboratory scale batch experimental data. The net energy versus interparticle distance for CeO_2 NPs in water and environmental systems were estimated using the Derjaguin, Landau, Verwey, Overbeek (DLVO) theory, i.e., the sum of van der Waals attraction and EDL repulsion between two approaching particles.

The novelty of this research consists of the analysis of the mechanisms governing the interfacial interactions between the surface of CeO_2 NPs as a function of pH, ionic composition, and Suwanee river humic and fulvic acids, the description and measurement of the dynamic growth of these nanoaggregate–CeO_2 complexes, and the evaluation of their colloidal stability in aqueous environment.

2. Materials and Methods

2.1. Materials

2.1.1. CeO_2 NP Stock Suspensions. CeO_2 NPs were obtained in the form of cerium (IV) oxide nanoparticles from Sigma–Aldrich (Saint Louis, MO). According to the manufacturer, the average particle size and density of CeO_2 NPs are below 25 nm and 7.13 g/cm^3 at 25°C, respectively. The particle size of CeO_2 NPs was obtained by application of the Brunauer, Emmett, and Teller (BET) theory, and the structural conformity of the CeO_2 NPs was measured by X-ray diffraction, as stated in the product information from Sigma–Aldrich. Every CeO_2 NP stock suspension (250 mg/L) was prepared according to the following dispersion protocol. First, a UMT2 ultramicrobalance (Mettler Toledo, Columbus, OH) in a Nano Enclosure Xpert®, 38,872 series (Labconco, Kansas City, MO) was used to weigh 250 mg of cerium (IV) oxide nanoparticles. Next, the weighted cerium oxide (IV) nanoparticles were dispersed in 80 mL ultrapure deionized (DI) water (18.2 MΩ cm) (Millipore Corporation, Billerica, MA) by ultrasonication, and diluted to a 1 L suspension. An ultrasonic liquid processor (S-4000, output power 600 W Max and output frequency 20 KHz, Misonix, Newton, CT) was used for the ultrasonication of the CeO_2 NP stock suspensions with the following settings: an amplitude of 45, a power of 45 W, and a sonication of 4 min.

2.1.2. HA and FA Stock Suspensions. Suwannee River humic acid (SRHA) (standard II, 2S101H) and Suwannee River fulvic acid (SRFA) (standard II, 2S101F) were obtained from the International Humic Substances Society, St. Paul, MN. A 50 mg/L SRHA stock suspension was first made by dissolving 50 mg of SRHA in 1 L of ultrapure DI water. A 1.41 mg/L of SRFA stock suspension was next prepared by dissolving 1.41 mg of SRFA powder in 1 L of ultrapure DI water. Both SRHA and SRFA suspensions were then filtered through Whatman™ hardened ashless filter papers, i.e., cotton filters made of high-quality cotton linters (Whatman quantitative filter paper, hardened ashless, Grade 542, GE Healthcare Life Sciences, Little Chalfont, UK) with nominal particle retention rating of 2.7 μm. The 50 mg/L SRHA and 1.41 mg/L SRFA suspensions were stored in the dark at 4°C in a refrigerator.

2.2. Preparation of CeO_2 NP Suspensions. CeO_2 NP stock suspension was sonicated in an ultrasonic bath (CPX2800H, Branson Ultrasonics Corporation, Danbury, CT) with settings of 110 W for power (maximum power) and 40 KHz for frequency for 30 min prior to use. A diluted CeO_2 NP suspension (25 mg/L) was obtained by mixing 10 mL of CeO_2 NP stock suspension with 90 mL of solution with specific IS in the absence and presence of SRHA or SRFA. The pH values, which ranged from 1 to 14 for the diluted CeO_2 NP suspensions (25 mg/L), were adjusted with HCl or NaOH (BDH®, VWR International, LLC, Radnor, PA) at different concentrations (0.01, 0.1, and 1 M) and measured with a FiveEasy™ Plus pH meter (Mettler-Toledo, Colombus, OH). Once the pH_{PZC} was determined from the analysis of the zeta potential measurements, two other pHs, which were above and below the pH_{PZC}, were selected for the later three pH region experiments.

Four concentrations (0.05, 0.1, 0.5, and 1 mM) and one control (0 mM) of NaCl (Fisher Scientific, Fair Lawn, NJ) and $CaCl_2$ (Amresco, Solon, OH) were prepared to obtain specific IS for each CeO_2 NP suspension. In addition, HA (5 mg/L) and FA (0.14 mg/L) were prepared using the specific IS concentration solutions (0, 0.1, and 1 mM) to obtain specific HS and IS conditions for each CeO_2 NP suspension.

Three pHs, greater than, equal to, and less than the pH_{PZC}, were then adjusted to obtain different pH–IS and pH–HS system suspensions. All the suspensions in the different pH–IS or pH–HS systems were prepared by diluting 250 mg/L CeO_2 NP stock suspension with specific IS or specific HS suspension and IS solution in 100 mL beakers employing a magnetic stirring system. The HCl and NaOH were used to adjust the pH of each suspension. The suspension was stirred until reaching the specific pH. All the suspensions were produced in four replicates (sets) for subsequent DLS and ELS analyses. A summary of the solution chemistry of the CeO_2 NP suspensions analyzed in this study is given in Table 1.

2.3. Aggregation Experiments. These diluted 25 mg/L CeO_2 NP suspensions were sonicated with the Misonix S-4000 ultrasonic liquid processor (50 amplitude and 45 W power) for 4 min before testing. A NanoBrook 90Plus Zeta Particle Size Analyzer (Brookhaven Instruments Corporation, Holtsville, NY) was used to characterize the aggregation behavior of the CeO_2 NPs. The maximum value of automatic measurements for each run in this analyzer's setting was 10 with manual operation required between two runs to obtain continuous data in approximately 1 hr. DLS was used to analyze the hydrodynamic diameters of CeO_2 NPs in one set of pH–IS or pH–HS system suspensions over approximately 1 hr. ELS also over an hour was then used to measure the zeta potentials of CeO_2 NPs in another set of both pH–IS and pH–HS system suspensions.

2.3.1. Particle Size Measurements. A NanoBrook 90Plus Zeta Particle Size Analyzer from Brookhaven Instruments Corporation (Holtsville, NY) was employed to analyze the particle size and to determine the hydrodynamic diameter of the CeO_2 nanoaggregates as a function of pH, ionic composition, SRHA, and SRFA. DLS measurements were used to establish the CeO_2 nanoaggregate sizes with the DLS measured by introducing the suspensions into BI-SCP plastic cells (10 W × 10 L × 52 H mm, 3.5 mL). Performed over a period of approximately 1 hr for each sample, the DLS was measured in an array of 31 runs, with each composed of 10 measurements with a 10 s time interval between them. The time separating the DLS runs was accounted for when reporting the DLS measurements. All DLS measurements were taken at 25°C.

2.3.2. Zeta Potential Measurements. A NanoBrook 90Plus Zeta Particle Size Analyzer from Brookhaven Instruments Corporation (Holtsville, NY) was employed to measure the zeta potential of the CeO_2 nanoaggregates with respect to pH, electrolytes, IS, SRHA, and SRFA. The zeta potential of the CeO_2 nanoaggregates was analyzed by placing 1.5 mL of the nanoparticles suspension in BI-SCP plastic cells followed by ELS measurements. The ELS was measured at 25°C for each sample within 1 hr to establish the zeta potential of these CeO_2 nanoaggregates. ELS measurements were taken continuously with the data collected and categorized every 10 min. The number of zeta potential measurements within 1 hr varied because the setting for data reading was observations of less than 0.05 relative residual. The time elapsing between the ELS runs was accounted for when reporting the ELS measurements. All ELS measurements were taken at 25°C.

2.4. Aggregation Kinetics Analysis. Nanoparticle aggregation kinetics were determined by monitoring the hydrodynamic radius α_h as a function of time (t). The initial rate of change of α_h was proportional to the initial aggregation rate constant k_{11}, as well as the initial particle concentration N_0, and expressed as follows:

$$\left(\frac{d\alpha_h(t)}{dt}\right)_{t\to 0} \propto k_{11}N_0. \quad (1)$$

The k_{11} was determined by using a linear correlation function to the experimental data during the early stage of aggregation (i.e., the first 600 s) [89–91]. The aggregation kinetics of each suspension were calculated using the data of the hydrodynamic radius of CeO_2 NPs obtained by DLS.

3. Results

3.1. Effect of pH on Stability of CeO_2 NPs. To establish the effect of pH on the stability of CeO_2 NPs, ELS, and DLS methods were used to measure the variation of surface charge and average hydrodynamic diameter. Figure 1 shows the average zeta potential and hydrodynamic diameter of CeO_2 NPs of approximately 1 hr measurements as a function of pH values ranging from extremely acidic (pH 1) to extremely basic (pH 14). The zeta potential of CeO_2 NPs was 10.28 ± 24.48 mV, and the average hydrodynamic diameter of CeO_2 NPs was 1,056.85 ± 345.63 nm at pH 1. When the pH of aqueous suspension changed from acidic to basic conditions (pH 2–12), the average zeta potential of CeO_2 NPs varied from positive values (e.g., 52.53 ± 10.26 mV at

Table 1: Solutions created for experimentation on the stability and aggregation of cerium oxide NPs in aqueous systems as a function of pH, electrolyte type and concentration, and the absence and presence of humic substances.

Systems				Humic substances					
				Humic acid 5 mg/L			Fulvic acid 0.14 mg/L		
	pH 8.2 + electrolyte concentration (mM)	pH 10.2 + electrolyte concentration (mM)	pH 12.2 + electrolyte concentration (mM)	pH 8.2 + electrolyte concentration (mM)	pH 10.2 + electrolyte concentration (mM)	pH 12.2 + electrolyte concentration (mM)	pH 8.2 + electrolyte concentration (mM)	pH 10.2 + electrolyte concentration (mM)	pH 12.2 + electrolyte concentration (mM)
DI water	0	0	0	0	0	0	0	0	0
				0.01	0.01	0.01	0.01	0.01	0.01
	0.05	0.05	0.05						
NaCl	0.1	0.1	0.1	0.1	0.1	0.1	0.1	0.1	0.1
	0.5	0.5	0.5						
	1	1	1	1	1	1	1	1	1
				0.01	0.01	0.01	0.01	0.01	0.01
	0.05	0.05	0.05						
$CaCl_2$	0.1	0.1	0.1	0.1	0.1	0.1	0.1	0.1	0.1
	0.5	0.5	0.5	1	1	1	1	1	1
	1	1	1						

These solutions include pH solutions ranging from 1 to 14, and aqueous systems with electrolytes (monovalent cation Na^+ at concentrations ranging from 0. to 1 mM, and divalent cation Ca^{2+} at concentrations ranging from 0 to 1 mM), at pH values of 8.2, 10.2, and 12.2, and in both the absence and presence of HA at 5 mg/L and FA at 0.14 mg/L.

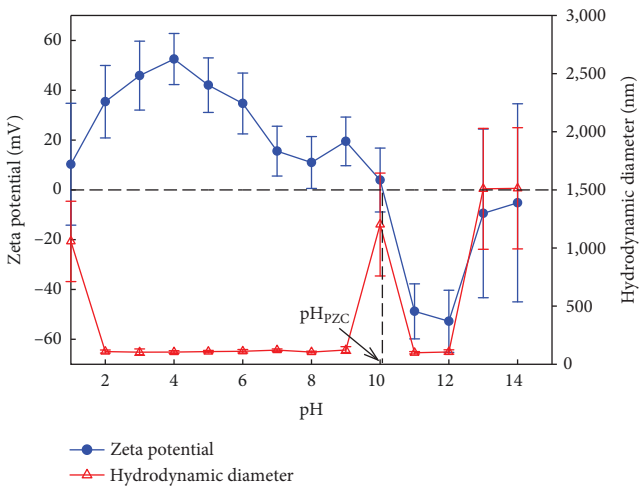

FIGURE 1: Zeta potential and hydrodynamic diameter of CeO_2 NPs as a function of pH (1–14). The results are presented as an average value of around 1 hr measurements with the corresponding standard deviation.

pH 4) to negative values (e.g., -52.76 ± 12.46 mV at pH 12), and the size of CeO_2 nanoaggregate was stable around 100 nm except at pH 10. The pH_{PZC} of CeO_2 NPs was 10.2, where the surface charge of CeO_2 NPs was neutralized, i.e., zeta potential was close to 0 mV. The CeO_2 NP nanoaggregate size increased significantly ($1{,}202.14 \pm 442.86$ nm) at pH 10, which was close to pH_{PZC} (Figure 1). Additionally, the hydrodynamic diameter reached about 1,500 nm, and the absolute average zeta potential was less than 10 mV at pH 13 and 14. Figure 2 presents results from the aggregation profiles, i.e., a series of aggregation experiments measuring the hydrodynamic diameters of CeO_2 NPs as a function of time by DLS, over pH values ranging from 1 to 14. After approximately 1 hr of incubation (i.e., ~1 hr), the CeO_2 NPs increased to the micron level at pH 1, 10, 13, and 14 (Figure 2). However, the hydrodynamic diameter of CeO_2 NPs was constant at other pH values (2–9 and 11–12) and close to 100 nm (Figure 2). The average hydrodynamic diameter of CeO_2 NPs during the first 100 s and at ~1 hr at pH ranging from 1 to 14 is displayed in Table S1. The size distribution represents the hydrodynamic diameter of NPs in different size ranges in order to analyze the size of NPs distributed at a time interval. The particle size distribution of CeO_2 NPs during the first 100 s and at ~1 hr at pH ranging from 1 to 14 is presented in Figure S1. The initial constant k_{11} aggregation rate represents the aggregation kinetics, which ranged between 0.80 and 1.50 nm/s at pH 1, 10, 13, and 14 (Figure 3). However, k_{11} was less than 0.10 nm/s at other pH values (2–9 and 11–12).

3.2. Impact of pH and NaCl on Stability of CeO_2 NPs. The effects of NaCl concentrations on CeO_2 NPs stability in three pH domains representing the three electrostatic states—$pH = 8.2 < pH_{PZC}$, $pH = 10.2 = pH_{PZC}$, and $pH = 12.2 > pH_{PZC}$—were examined by measuring the surface charge and size of nanoparticles using ELS and DLS methods.

3.2.1. Positively Charged CeO_2 NPs in the Presence of NaCl ($pH = 8.2 < pH_{PZC}$). The aggregation experiments were conducted at pH 8.2 ($pH < pH_{PZC}$), where CeO_2 NPs were positively charged in the absence of NaCl (Figure 1). The aggregation profiles and average zeta potentials of CeO_2 NPs at pH value of 8.2 and in the presence of monovalent NaCl salt at various concentrations are presented in Figures 4(a) and 4(b) and Figures 5(a) and 5(b), respectively.

The surface charge reflects the inclination of aggregation or stabilization of NPs. In terms of time, the surface charge of CeO_2 NPs in the presence of NaCl at each NaCl concentration at each 10 min interval in 1 hr was relatively stable. It is independent of time at $pH < pH_{PZC}$ (Figures 5(a) and 5(b) and Table S2). However, when considering the concentration of NaCl, the zeta potential decreased from around 21 mV to around 10 mV when the concentration of NaCl augmented from 0 to 1 mM. The Pearson's correlation coefficients for the ξ potential values of CeO_2 NPs and time at pH 8.2 in concentration of NaCl 0, 0.05, 0.1, 0.5, and 1 mM are 0.10, 0.84, −0.28, 0.56 and −0.76, respectively.

The results of hydrodynamic diameter measurements were the same as predicted by the results of surface charge. CeO_2 NPs were stable at $pH < pH_{PZC}$ when the concentration of NaCl was less than 1 mM (Figures 4(a) and 4(b)). When concentration of NaCl reached 1 mM, the hydrodynamic diameter of CeO_2 NPs in about 1 hr increased rapidly by 122.28% during the first 100 s (188.74 ± 29.89 nm) and 1,098.98% ($1{,}346.21 \pm 221.29$ nm) at ~1 hr, when compared to the controls during the first 100 s (84.91 ± 3.61 mm) and at ~1 hr (112.28 ± 2.11 mm), respectively (Table S3). The particle size distribution of CeO_2 NPs during the first 100 s and at ~1 hr at pH value of 8.2 and in the presence of monovalent NaCl salt at various concentrations is presented in Figures S2(a) and S2(b).

The aggregation rate constant k_{11} an indicator of the stability of NPs under different conditions is obtained by using linear regression of hydrodynamic radius over 10 min in this experiment. The results of k_{11} also show the same prediction as surface charge measurements. The k_{11} was 0.35 nm/s at 1 mM NaCl, which was larger than values (<0.02 nm/s) at other NaCl concentrations (Table 2).

The net energy barrier is also an indicator of the stability of NPs. The larger net energy barrier means more stable NPs, while no barrier indicates the inclination of the aggregation of NPs. The results show that the net energy barrier disappeared at 1 mM NaCl (Figure 6(a)), which is the same prediction as surface charge and hydrodynamic diameter measurements of CeO_2 NPs.

3.2.2. Uncharged CeO_2 NPs in the Presence of NaCl ($pH = 10.2 = pH_{PZC}$). At $pH = pH_{PZC}$, the surface of CeO_2 NPs is neutralized in the absence of NaCl (Figure 1). The aggregation profiles and average zeta potentials of CeO_2 NPs at pH 10.2 and in the presence of monovalent NaCl salt at various concentrations are presented in Figures 4(c) and 4(d) and Figures 5(c) and 5(d), respectively.

In the presence of NaCl, the absolute average zeta potential of CeO_2 NPs varied around 0 mV and was less than

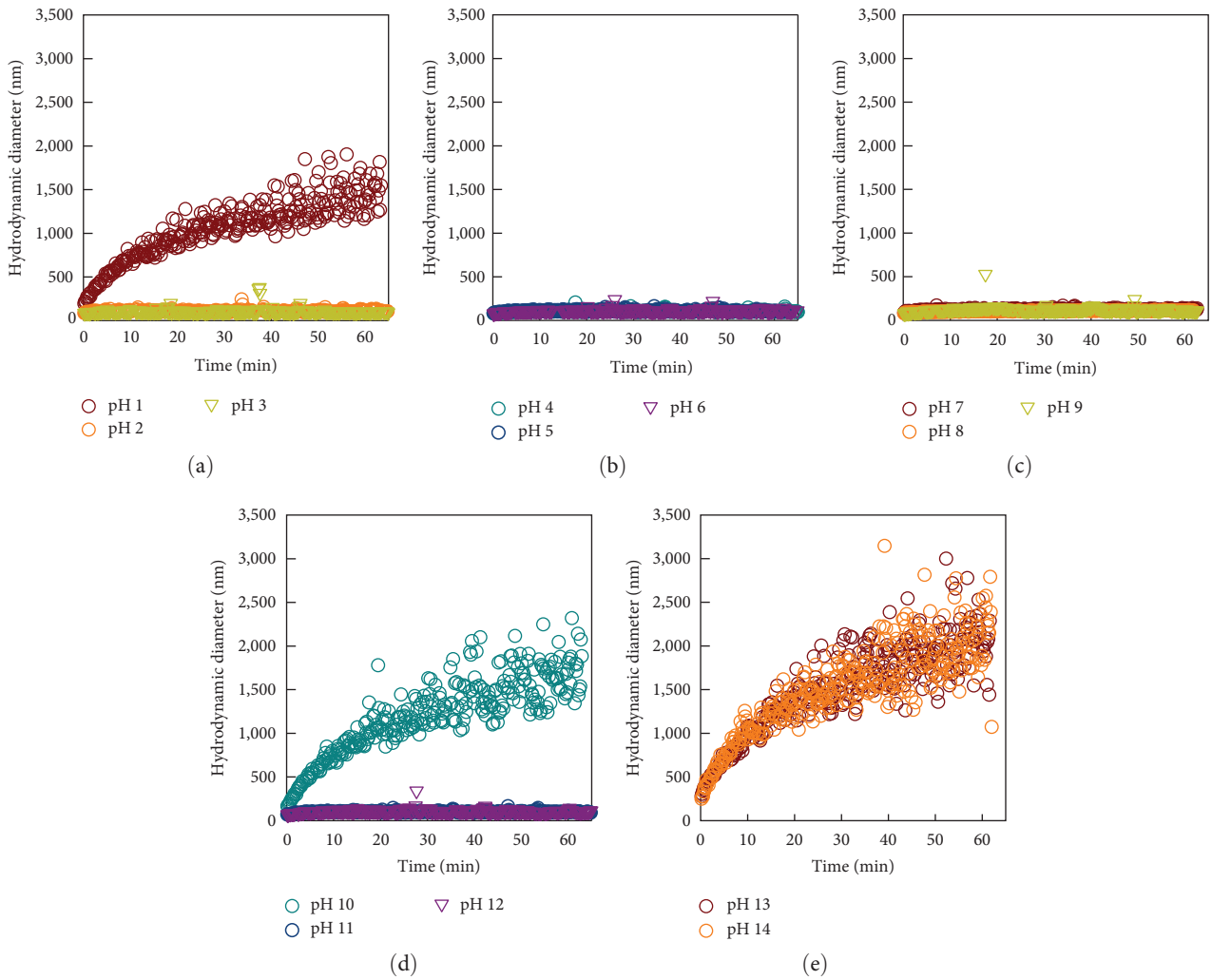

FIGURE 2: Hydrodynamic diameter of CeO_2 NPs as function of pH (1–14) over about 1 hr: (a) pH 1–3, (b) pH 4–6, (c) pH 7–9, (d) pH 10–12, and (e) pH 13 and 14.

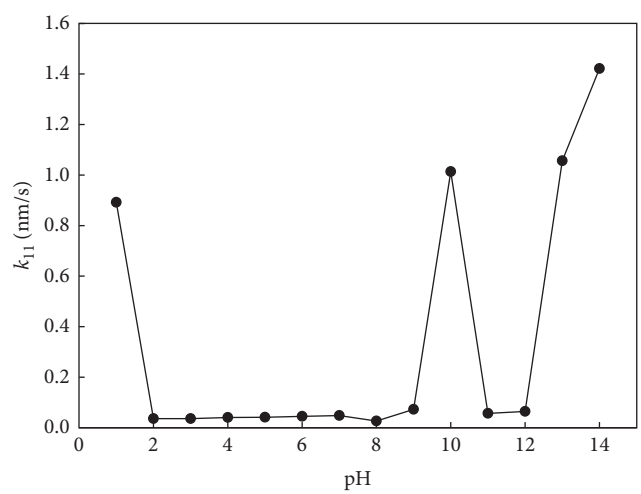

FIGURE 3: Initial aggregation rate constant k_{11} of CeO_2 NPs as a function of pH (1–14) during the first 600 s.

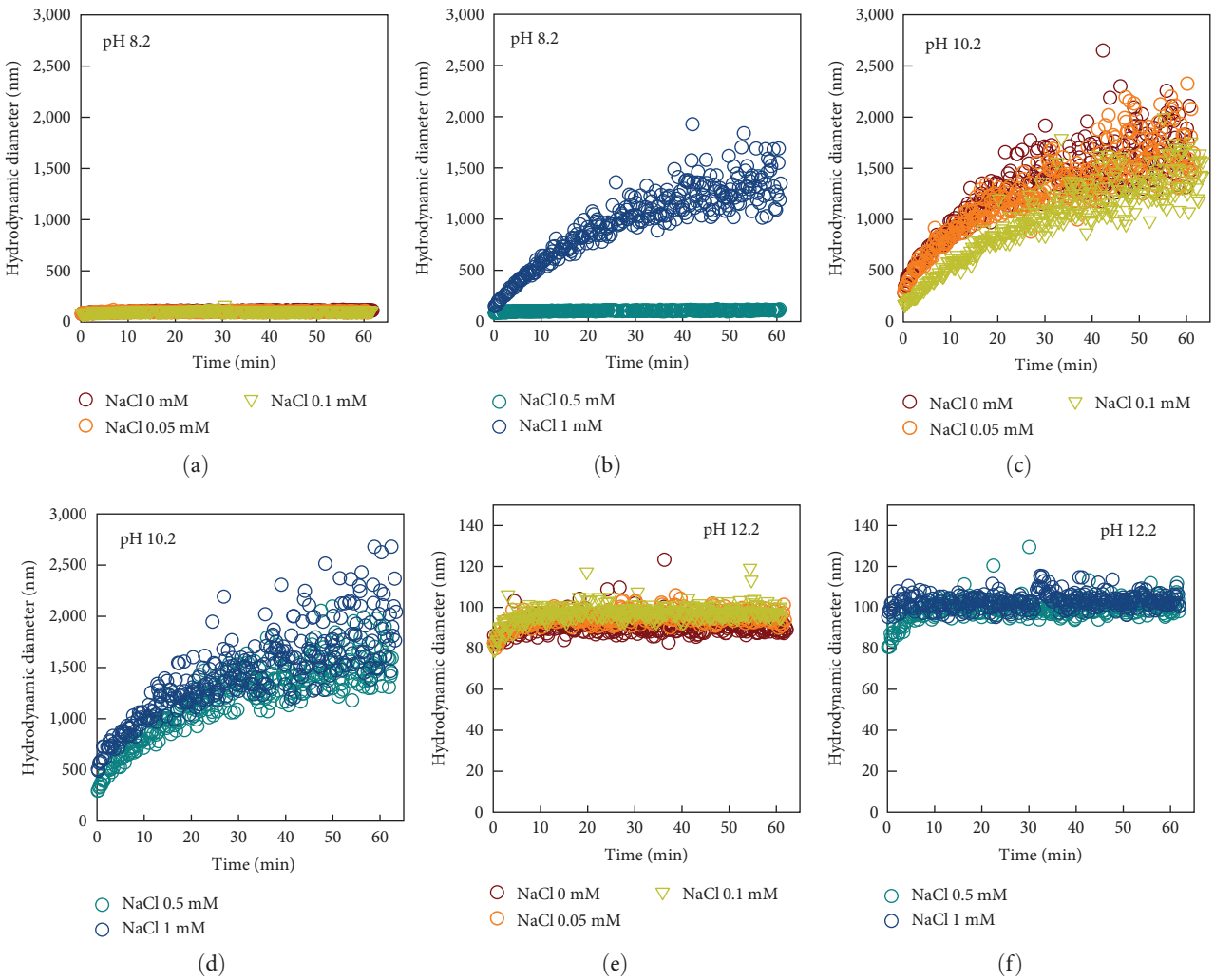

FIGURE 4: Hydrodynamic diameter of CeO_2 NPs as function of time in varying concentrations of NaCl ranging from 0 to 1 mM at pH 8.2, pH 10.2, and pH 12.2: (a) 0, 0.05, and 0.1 mM NaCl and pH 8.2; (b) 0.5 and 1 mM NaCl and pH 8.2; (c) 0, 0.05, and 0.1 mM NaCl and pH 10.2; (d) 0.5 and 1 mM NaCl and pH 10.2; (e) 0, 0.05, and 0.1 mM NaCl and pH 12.2; (f) 0.5 and 1 mM NaCl and pH 12.2.

20 mV (Figures 5(c) and 5(d) and Table S2). However, the surface charge of CeO_2 NPs was negative at 0, 0.05, and 1 mM of NaCl, but positive at 0.1 and 0.5 mM of NaCl. The surface charge is independent of time at $pH = pH_{PZC}$. The Pearson's correlation coefficients for the ξ potential values of CeO_2 NPs and time at pH 10.2 in concentration of NaCl 0, 0.05, 0.1, 0.5, and 1 mM are −0.76, −0.48, −0.79, −0.67 and 0.61, respectively. The results of hydrodynamic diameter, k_{11}, size distribution, and net energy barrier were the same as the prediction from the surface charge results, which suggests that CeO_2 NPs were unstable in the presence of NaCl at $pH = pH_{PZC}$. The hydrodynamic diameter of CeO_2 NPs under all the NaCl concentrations grew at high rates and reached several microns after approximately 1 hr of incubation, at ∼1 hr (Figures 4(c) and 4(d)). For example, the hydrodynamic diameter of CeO_2 NPs at 0.1 mM NaCl increased by 618.28% at ∼1 hr (1,430.52 ± 159.61 nm) when compared to the hydrodynamic diameter during the first 100 s (199.16 ± 23.37 nm) (Table S3). The particle size distribution of CeO_2 NPs during the first 100 s and at ∼1 hr at pH value of 10.2 and in the presence of monovalent NaCl salt at various concentrations is presented in Figures S2(c) and S2(d). The k_{11} under all the NaCl concentrations (0.33–0.45 nm/s) was greater than that at pH 8.2 and pH 12.2, and no concentration-dependent increase was observed (Table 2). No energy barriers were present when the Na^+ concentration was larger than 0.1 mM (Figure 6(b)).

3.2.3. Negatively Charged CeO_2 NPs in the Presence of NaCl ($pH = 12.2 > pH_{PZC}$). At pH = 12.2 ($pH > pH_{PZC}$), the CeO_2 NPs exhibited negative zeta potential values in the absence of NaCl (Figure 1). The aggregation profiles and average zeta potentials of CeO_2 NPs at pH value of 8.2 and in the presence of monovalent NaCl salt at various concentrations are presented in Figures 4(e) and 4(f) and Figures 5(e) and 5(f), respectively.

In the presence of NaCl, the average zeta potential of CeO_2 NPs in 1 hr (0–60 min) was less than −30 mV (Figures 5(e) and 5(f) and Table S2). This finding indicates that CeO_2 NPs are stable at $pH > pH_{PZC}$, which is also demonstrated by the results of hydrodynamic diameter, size distribution, and net energy

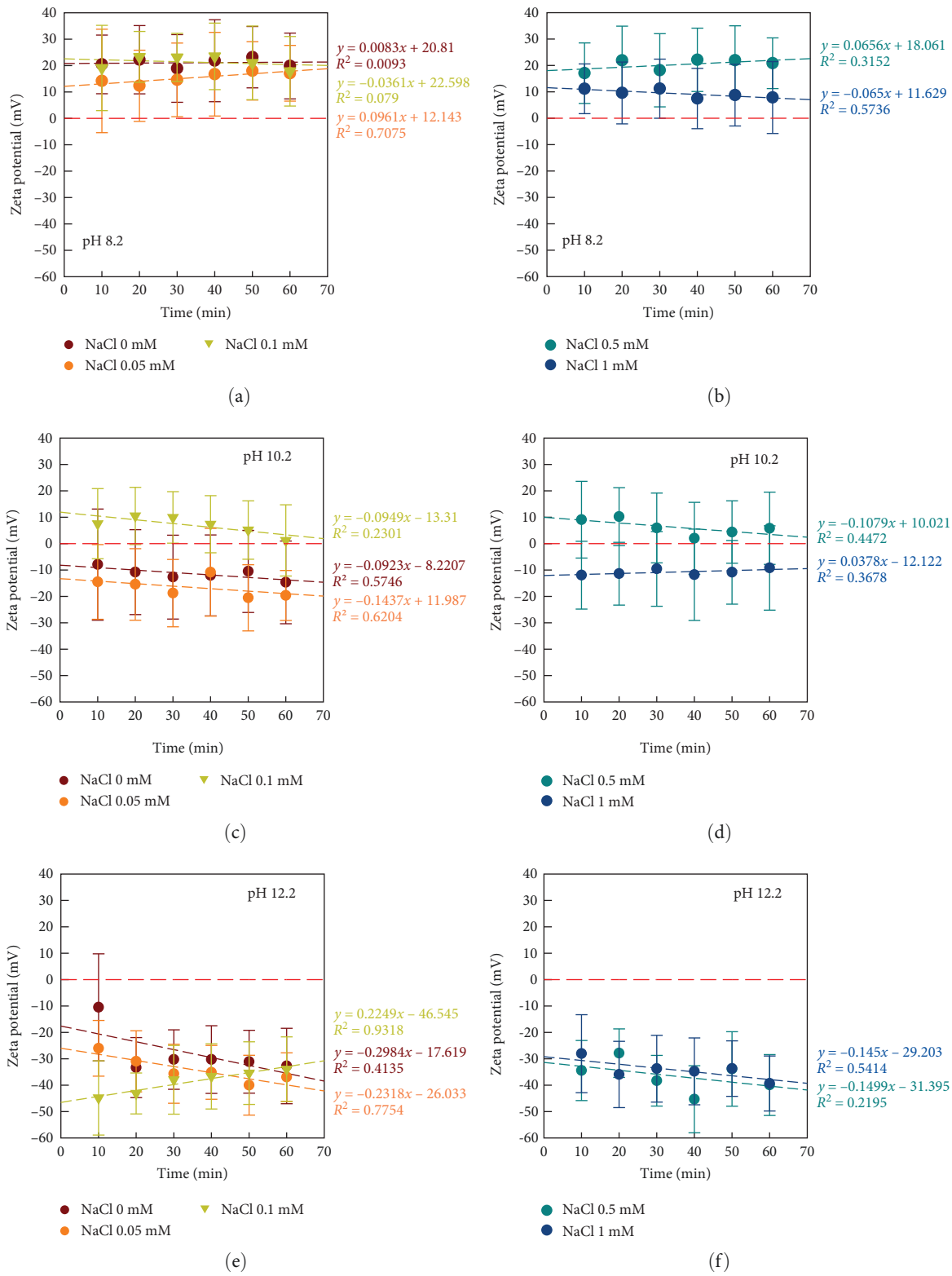

Figure 5: Zeta potential of CeO_2 NPs as function of time in varying concentrations of NaCl ranging from 0 to 1 mM at pH 8.2, pH 10.2, and pH 12.2: (a) 0, 0.05 and 0.1 mM NaCl, and pH 8.2; (b) 0.5 and 1 mM NaCl, and pH 8.2; (c) 0, 0.05 and 0.1 mM NaCl, and pH 10.2; (d) 0.5 and 1 mM NaCl, and pH 10.2; (e) 0, 0.05 and 0.1 mM NaCl, and pH 12.2; (f) 0.5 and 1 mM NaCl, and pH 12.2.

Table 2: Initial aggregation rate constant k_{11} obtained from the linear regression of the experimental data during the first 600 s, under varying concentrations of NaCl or $CaCl_2$ ranging from 0 to 1 mM in the absence and presence of HA (5 mg/L) or FA (0.14 mg/L) at three different pH values (8.2, 10.2, and 12.2).

pH	Electrolyte concentration (mM)	Aggregation rate (nm/s)					
		NaCl	$CaCl_2$	HA		FA	
				NaCl	$CaCl_2$	NaCl	$CaCl_2$
	0.00	0.01	0.01	0.51	0.51	0.02	0.02
	0.05	0.01	0.01				
8.2	0.10	0.02	0.01	0.01	0.04	0.01	0.02
	0.50	0.02	0.01				
	1.00	0.35	0.08	0.25	0.11	0.02	0.02
	0.00	0.44	0.44	0.54	0.54	0.02	0.02
	0.05	0.45	0.25				
10.2	0.10	0.33	0.35	0.42	0.37	0.01	0.01
	0.50	0.40	0.41				
	1.00	0.44	0.50	0.48	0.44	0.02	0.02
	0.00	0.01	0.01	0.01	0.01	0.02	0.02
	0.05	0.01	0.02				
12.2	0.10	0.01	0.02	0.02	0.02	0.01	0.01
	0.50	0.01	0.47				
	1.00	0.00	0.00	0.02	0.00	0.01	0.02

barrier. The Pearson's correlation coefficients for the ξ potential values of CeO_2 NPs and time at pH 12.2 in concentration of NaCl 0, 0.05, 0.1, 0.5, and 1 mM are −0.64, −0.88, 0.97, −0.47, and −0.74, respectively. The hydrodynamic diameter of CeO_2 NPs at this pH grew at low rates for all NaCl concentrations (Figures 4(e) and 4(f)). For all NaCl concentrations, the average hydrodynamic diameter of CeO_2 NPs was less than 110 nm after approximately 1 hr of incubation, at ∼1 hr. For example, the hydrodynamic diameter of CeO_2 NPs at 0.5 mM NaCl increased by only 19.87% at ∼1 hr (102.39 ± 4.81 nm) when compared to the hydrodynamic diameter during the first 100 s (85.42 ± 3.99 nm) (Table S4). The particle size distribution of CeO_2 NPs during the first 100 s and at ∼1 hr at pH value of 12.2 and in the presence of monovalent NaCl salt at various concentrations is presented in Figures S2(e) and S2(f). The k_{11} was very small (less than 0.02 nm/s) for concentrations of NaCl ranging from 0 to 1 mM (Table 2). The energy barriers were 3.10, 6.00, 4.73, and 2.30 kJ, for 0.05, 0.1, 0.5 and 1 mM of Na^+, respectively (Figure 6(c)).

3.3. Impact of pH and $CaCl_2$ on Stability of CeO_2 NPs. The effects of $CaCl_2$ concentrations on CeO_2 NPs stability in three pH domains representing the three electrostatic states—$pH = 8.2 < pH_{PZC}$, $pH = 10.2 = pH_{PZC}$, and $pH = 12.2 > pH_{PZC}$—were examined by measuring the surface charge and size of nanoparticles using ELS and DLS methods.

3.3.1. Positively Charged CeO_2 NPs in the Presence of $CaCl_2$ ($pH = 8.2 < pH_{PZC}$). The aggregation profiles and average zeta potentials of CeO_2 NPs at pH value of 8.2 and in the presence of divalent $CaCl_2$ salt at various concentrations are given in Figures 7(a) and 7(b) and Figures 8(a) and 8(b), respectively. At pH 8.2 ($pH < pH_{PZC}$), at 0–10 min, the average zeta potential of CeO_2 NPs diminished from 20.46 ± 11.12 mV to 16.21 ± 11.37 mV when the concentration increased from 0 to 0.1 mM of $CaCl_2$, but it then increased to 21.41 ± 13.45 mV when the $CaCl_2$ concentration raised to 1 mM (Figures 8(a) and 8(b) and Table S2). However, the manifestation of different trends occurred at 50–60 min. At this point, the average zeta potential increased from 19.88 ± 12.47 mV to 27.65 ± 7.76 mV with the increase of $CaCl_2$ concentration (increased from 0 to 0.1 mM). It then decreased to 12.71 ± 13.08 mV when the concentration of $CaCl_2$ was 0.5 mM, and increased to 22.40 ± 7.50 mV when the $CaCl_2$ concentration was 1 mM. The Pearson's correlation coefficients for the ξ potential values of CeO_2 NPs and time at pH 8.2 in concentration of $CaCl_2$ 0, 0.05, 0.1, 0.5, and 1 mM are 0.10, 0.92, 0.82, −0.85, and 0.60, respectively. No obvious prediction was possible from the results of zeta potential when CeO_2 NPs were in the presence of $CaCl_2$ at pH 8.2.

The hydrodynamic diameter of CeO_2 NPs was greater at 1 mM $CaCl_2$ than at other $CaCl_2$ concentrations (Figures 7(a) and 7(b)). At ∼1 hr, the average hydrodynamic diameter at 1 mM $CaCl_2$ (922.91 ± 89.41 nm) was 721.97% (112.28 ± 2.11 nm), 763.99% (106.82 ± 2.29 nm), 615.05% (129.07 ± 5.38 nm), and 426.62% (175.25 ± 11.86 nm) greater than at 0, 0.05, 0.1, and 0.5 mM $CaCl_2$, respectively (Table S3). This finding indicates that CeO_2 NPs are unstable at 1 mM $CaCl_2$. The particle size distribution of CeO_2 NPs during the first 100 s and at ∼1 hr at pH value of 8.2 and in the presence of monovalent $CaCl_2$ salt at various concentrations is presented in Figures S3(a) and S3(b). The same prediction can be demonstrated by k_{11} and size distribution. When the concentration of $CaCl_2$ was less than 1 mM, k_{11} was very small (0.01 nm/s) (Table 2). At 1 mM $CaCl_2$, k_{11} increased to 0.08 nm/s.

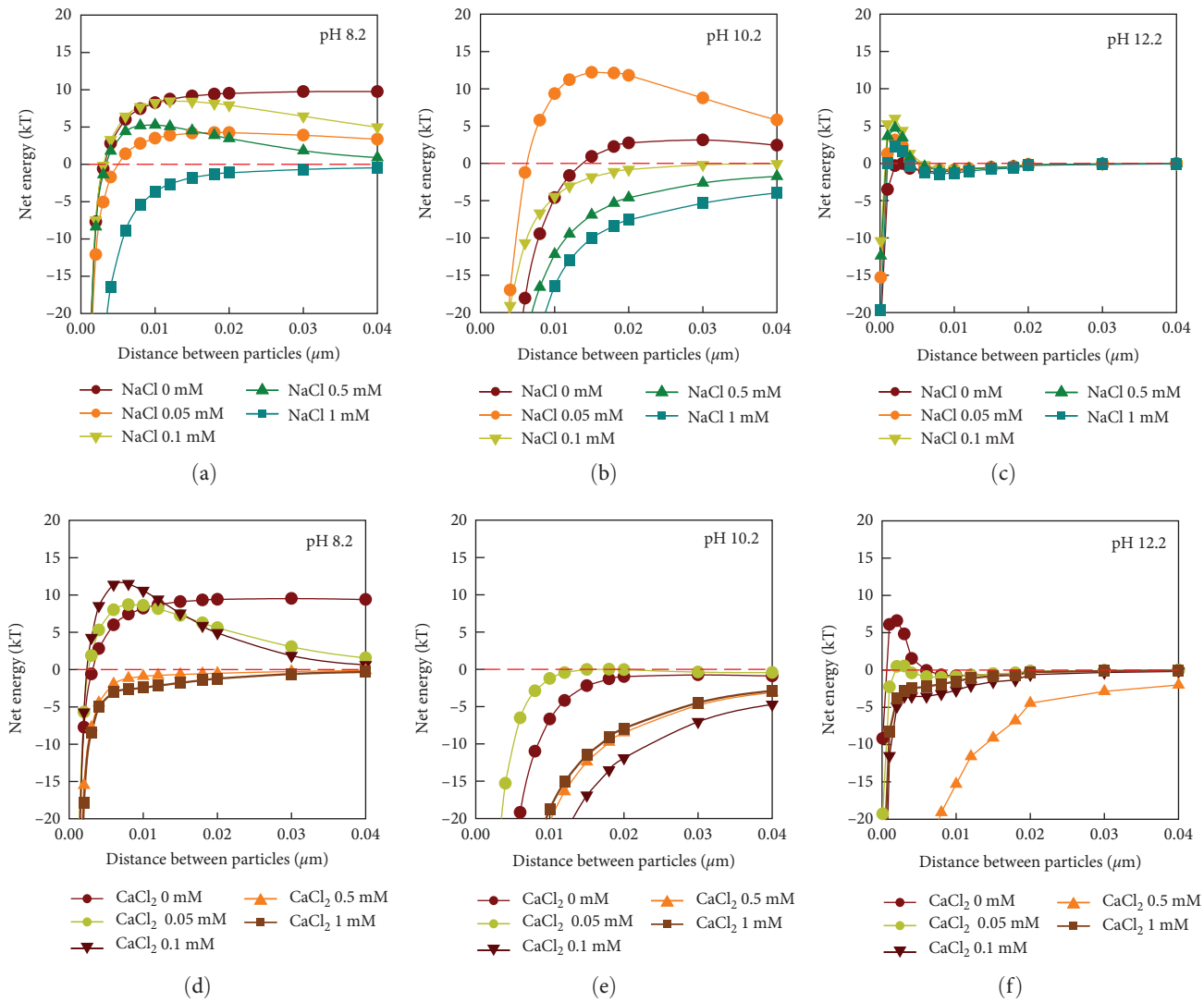

FIGURE 6: Net energy versus interparticle distance according to DLVO theory, showing the influence of representative monovalent electrolyte NaCl or divalent electrolyte $CaCl_2$ concentrations varying from 0 to 1 mM at pH 8.2, pH 10.2, and pH 12.2, for CeO_2 NPs suspended in aqueous systems: (a) NaCl and pH 8.2; (b) NaCl and pH 10.2; (c) NaCl and pH 12.2; (d) $CaCl_2$ and pH 8.2; (e) $CaCl_2$ and pH 10.2; and (f) $CaCl_2$ and 12.2. Calculation of DLVO theory includes the contributions of the van der Waals and electric double layer (EDL) interactions. The net energy (Net) shown is the sum of EDL repulsion and van der Waals attraction between two approaching particles.

However, the prediction from the result of hydrodynamic diameter differed little from the prediction from the net energy analysis, possibly affected by the values of both the zeta potential and IS. The net energy barrier disappeared at 0.5 and 1 mM of $CaCl_2$ (Figure 6(d)). This absence indicates that the CeO_2 NPs are stable when the concentration of $CaCl_2$ is less than 0.5 mM, but unstable when the concentration of $CaCl_2$ reaches 0.5 and 1 mM.

3.3.2. Uncharged CeO_2 NPs in the Presence of $CaCl_2$ (pH = 10.2 = pH_{PZC}). The aggregation profiles and average zeta potentials of CeO_2 NPs at pH value of 10.2 and in the presence of divalent $CaCl_2$ salt at various concentrations are shown in Figures 7(c) and 7(d) and Figures 8(c) and 8(d). At pH 10.2 (pH = pH_{PZC}), the average zeta potential of CeO_2 NPs in the presence of $CaCl_2$ varied about 0 mV (Figures 8(c) and 8(d) and Table S2), which indicates that CeO_2 NPs are unstable and the surface charge of CeO_2 NPs is independent of time at pH = pH_{PZC}. The Pearson's correlation coefficients for the ξ potential values of CeO_2 NPs and time at pH 10.2 in concentration of $CaCl_2$ 0, 0.05, 0.1, 0.5, and 1 mM are −0.76, −0.62, −0.83, −0.73, and −0.40, respectively. The unstabilty prediction of CeO_2 NPs at pH = pH_{PZC} is also demonstrated by the results of hydrodynamic diameter, k_{11}, size distribution, and net energy barrier. At pH 10.2, hydrodynamic diameters under all the $CaCl_2$ concentrations grew at very high rates (Figures 7(c) and 7(d)). At ∼1 hr, the average hydrodynamic diameters were 1,670.11 ± 229.21 nm, 1,318.10 ± 125.18 nm, 1,690.85 ± 210.69 nm, 1,845.22 ± 175.04 nm, and 3,568.23 ± 552.86 nm, at 0, 0.05, 0.1, 0.5, and 1 mM of $CaCl_2$, respectively (Table S3). For example, the hydrodynamic diameter of CeO_2 NPs at 0.1 mM $CaCl_2$ increased by 167.77% at ∼1 hr

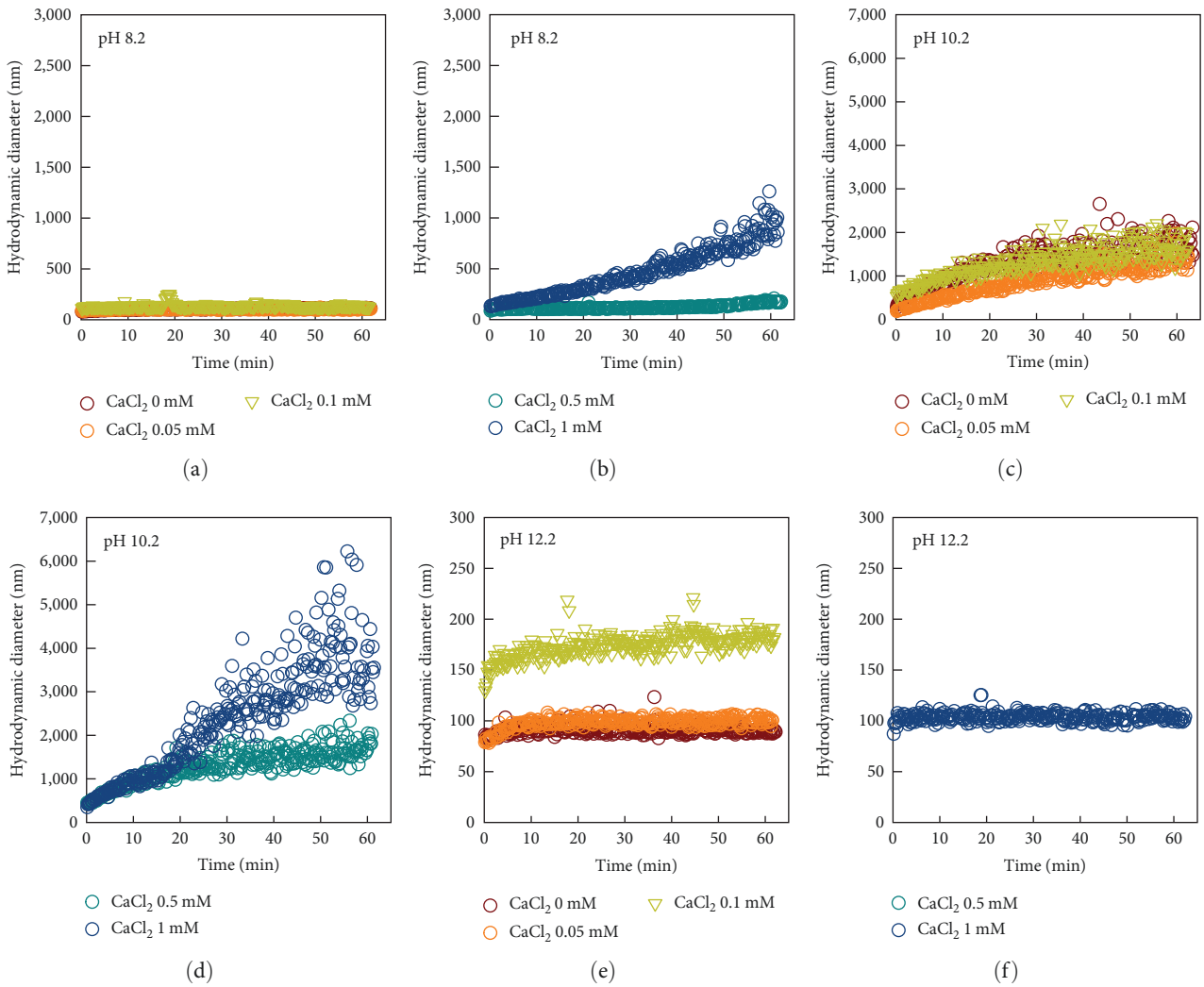

FIGURE 7: Hydrodynamic diameter of CeO_2 NPs as function of time in varying concentrations of $CaCl_2$ ranging from 0 to 1 mM at pH 8.2, pH 10.2, and pH 12.2: (a) 0, 0.05, and 0.1 mM $CaCl_2$ and pH 8.2; (b) 0.5 and 1 mM $CaCl_2$ and pH 8.2; (c) 0, 0.05, and 0.1 mM $CaCl_2$ and pH 10.2; (d) 0.5 and 1 mM $CaCl_2$ and pH 10.2; (e) 0, 0.05, and 0.1 mM $CaCl_2$ and pH 12.2; and (f) 0.5 and 1 mM $CaCl_2$, and pH 12.2.

(1,690.85 ± 210.69 nm) when compared to the hydrodynamic diameter during the first 100 s (631.45 ± 49.47 nm). The particle size distribution of CeO_2 NPs during the first 100 s and at ∼1 hr at pH value of 10.2 and in the presence of monovalent $CaCl_2$ salt at various concentrations is presented in Figures S3(c) and S3(d). k_{11} in the presence of $CaCl_2$ was 0.25–0.50 nm/s at pH 10.2 (Table 2), which was greater than at pH 8.2 and 12.2. No energy barrier was present at pH 10.2 (Figure 6(e)).

3.3.3. Negatively Charged CeO_2 NPs in the Presence of $CaCl_2$ ($pH = 12.2 > pH_{PZC}$). The aggregation profiles and average zeta potentials of CeO_2 NPs at pH value of 12.2 and in the presence of divalent $CaCl_2$ salt at various concentrations are shown in Figures 7(e) and 7(f) and Figures 8(e) and 8(f), respectively. At pH 12.2 ($pH > pH_{PZC}$), the average zeta potential in 1 hr was approximately −30 mV at 0, 0.05, 0.1, and 1 mM $CaCl_2$ (Figures 8(e) and 8(f) and Table S2). However, the zeta potential in 1 hr was −5.65 ± 20.67 mV at 0.5 mM $CaCl_2$. The Pearson's correlation coefficients for the ξ potential values of CeO_2 NPs and time at pH 12.2 in concentration of $CaCl_2$ 0, 0.05, 0.1, 0.5, and 1 mM are −0.64, −0.86, −0.25, 0.13, and −0.91, respectively. This finding indicates that although CeO_2 NPs were unstable at 0.5 mM $CaCl_2$, they remained stable at other $CaCl_2$ concentrations. The same prediction was obtained from the results of the other three parameters, which are the hydrodynamic diameter, k_{11}, and the size distribution.

At pH 12.2 ($pH > pH_{PZC}$), the growth rates were low for all $CaCl_2$ concentrations, except for 0.5 mM of $CaCl_2$ (Figures 7(e) and 7(f)). At ∼1 hr, the average hydrodynamic diameters were 89.09 ± 1.56 nm, 99.74 ± 2.37 nm, 182.14 ± 5.52 nm, 1,700.32 ± 287.78 nm, and 101.85 ± 2.72 nm under 0, 0.05, 0.1, 0.5, and 1 mM of $CaCl_2$, respectively (Table S3). This finding demonstrates that CeO_2 NPs in the presence of $CaCl_2$ are stable at $pH > pH_{PZC}$, except for 0.5 mM of $CaCl_2$. For example, the hydrodynamic diameter of CeO_2 NPs at 1 mM $CaCl_2$ increased only by 2.64% at ∼1 hr (101.85 ± 2.72 nm)

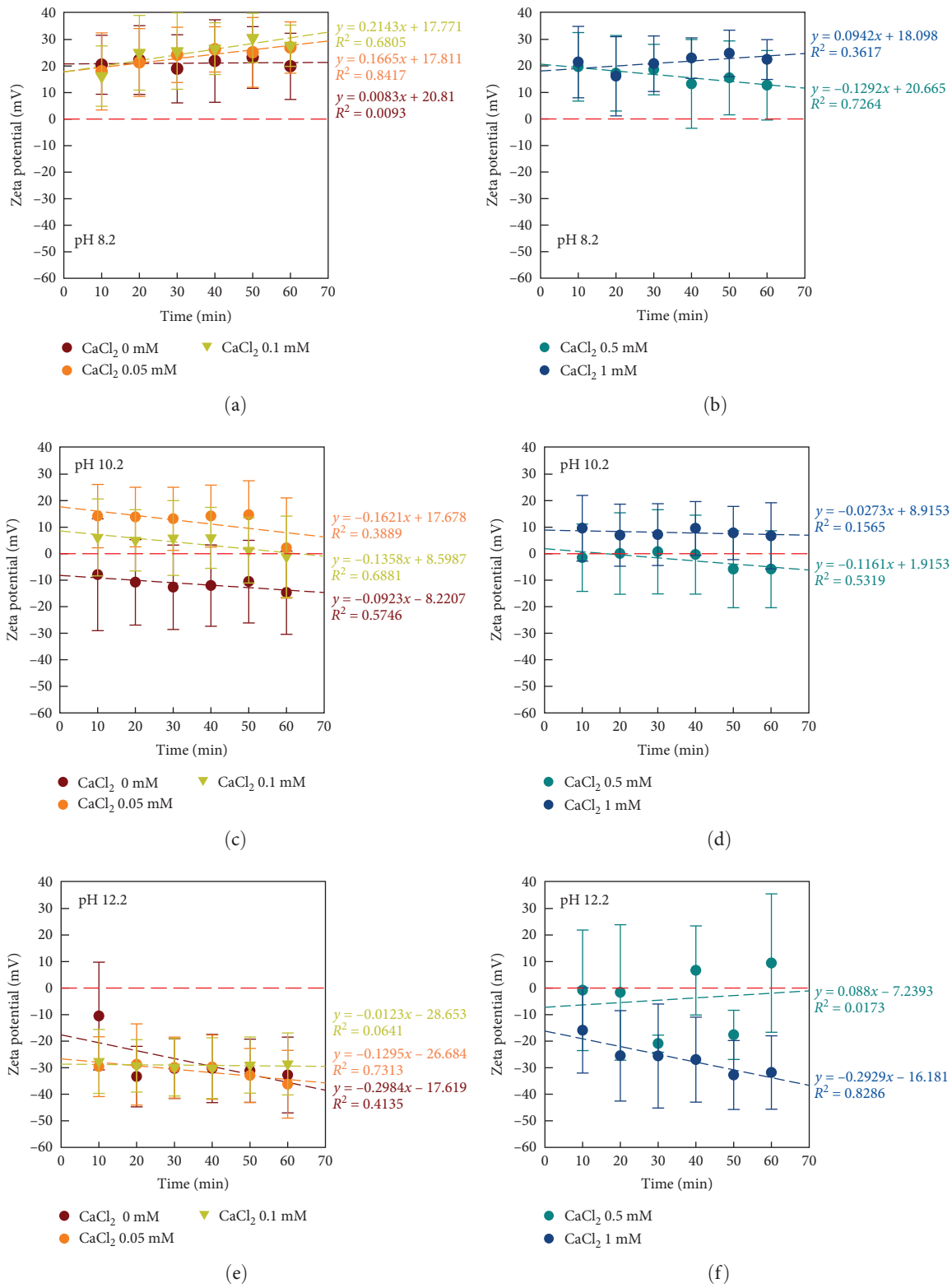

FIGURE 8: Zeta potential of CeO_2 NPs as function of time in varying concentrations of $CaCl_2$ ranging from 0 to 1 mM at pH 8.2, pH 10.2, and pH 12.2: (a) 0, 0.05, and 0.1 mM $CaCl_2$ and pH 8.2; (b) 0.5 and 1 mM $CaCl_2$ and pH 8.2; (c) 0, 0.05, and 0.1 mM $CaCl_2$ and pH 10.2; (d) 0.5 and 1 mM $CaCl_2$ and pH 10.2; (e) 0, 0.05, and 0.1 mM $CaCl_2$ and pH 12.2; and (f) 0.5 and 1 mM $CaCl_2$ and pH 12.2.

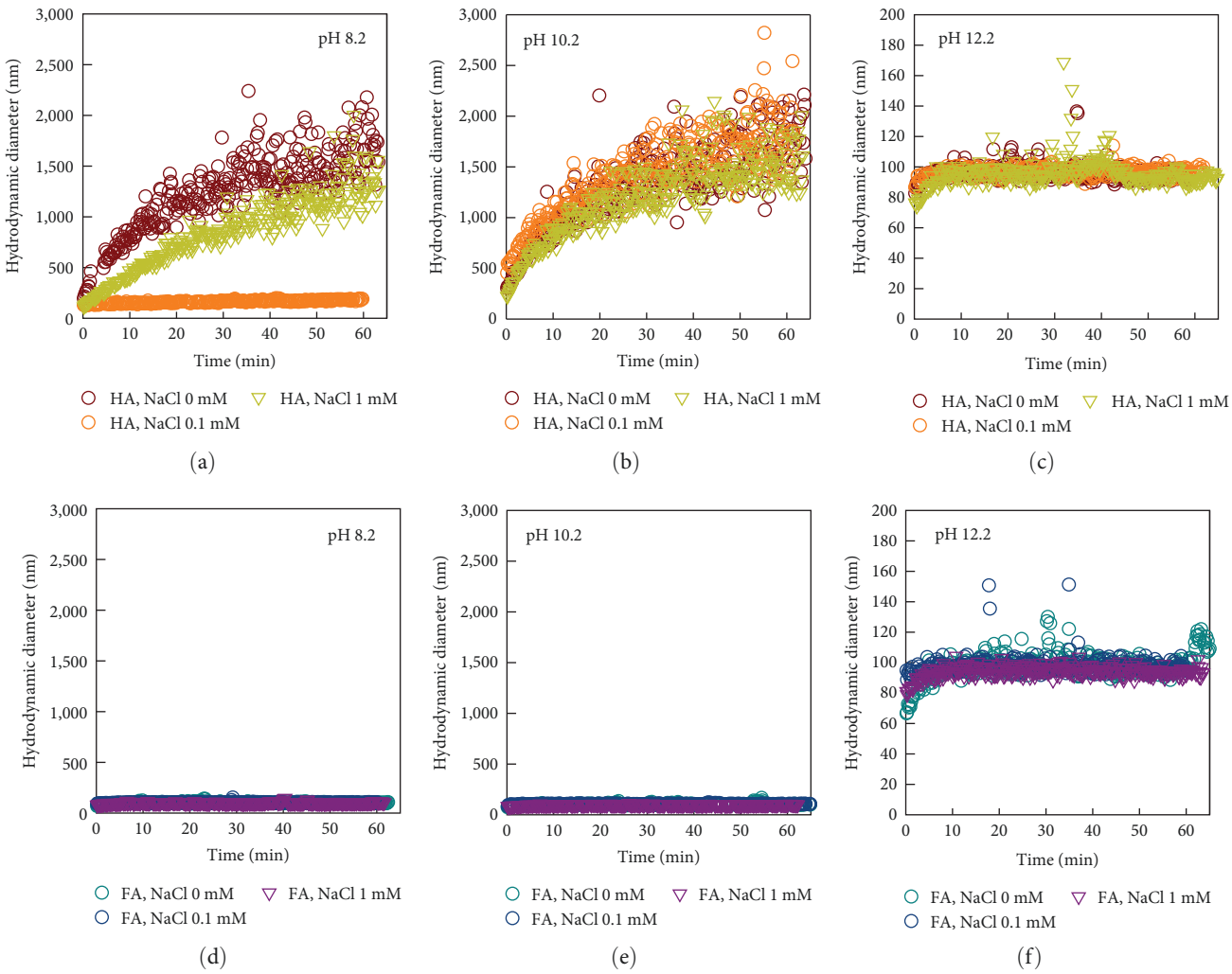

Figure 9: Hydrodynamic diameter measurements of CeO_2 NPs in the presence of HA (5 mg/L) or FA (0.14 mg/L) as a function of time, and NaCl concentration ranging from 0 to 1 mM at pH 8.2, pH 10.2, and pH 12.2: (a) HA, NaCl, and pH 8.2; (b) HA, NaCl, and pH 10.2; (c) HA, NaCl, and pH 12.2; (d) FA, NaCl, and pH 8.2; (e) FA, NaCl, and pH 10.2; and (f) FA, NaCl, and pH 12.2.

when compared to the hydrodynamic diameter during the first 100 s (99.23 ± 5.87 nm). The particle size distribution of CeO_2 NPs during the first 100 s and at ~1 hr at pH value of 12.2 and in the presence of monovalent $CaCl_2$ salt at various concentrations is presented in Figures S3(e) and S3(f). The k_{11} was very low (<0.02 nm/s) at 0, 0.05, 0.1, and 1 mM $CaCl_2$ (Table 2). However, k_{11} was 0.47 nm/s at 0.5 mM $CaCl_2$. The values of energy barriers were 6.60 and 0.51 kJ, for 0 and 0.05 mM $CaCl_2$, respectively (Figure 6(f)). However, the prediction from all the parameters above differed from the prediction from the result of the net energy barrier at 0.1 and 1 mM of $CaCl_2$. No energy barrier was found for 0.1, 0.5, and 1 mM of $CaCl_2$.

3.4. Impact of pH and HA on Stability of CeO_2 NPs. The effects of HA and cation (Na^+ and Ca^{2+}) concentrations on CeO_2 NPs stability in three pH domains representing the three electrostatic states (i.e., $pH = 8.2 < pH_{PZC}$, $pH = 10.2 = pH_{PZC}$, and $pH = 12.2 > pH_{PZC}$) were examined via ELS and DLS measurements of the nanoparticle surface charges and sizes.

3.4.1. Positively Charged CeO_2 NPs in the Presence of HA ($pH = 8.2 < pH_{PZC}$). The aggregation profiles and average zeta potentials of CeO_2 NPs at pH value of 8.2 and in the presence of monovalent NaCl or divalent $CaCl_2$ salts as well as SRHA, all at various concentrations, are given in Figures 9(a) and 10(a) and Figures 11(a) and 11(b), respectively. At pH 8.2 ($pH < pH_{PZC}$), at 0–60 min, in the presence of HA, when the concentration of NaCl increased from 0 to 1 mM, the average zeta potential of CeO_2 NPs increased from 7.98 ± 20.71 mV to 13.03 ± 9.68 mV (Figures 11(a) and 11(b) and Table S2). However, it increased initially when the $CaCl_2$ concentration increased from 0 to 0.01 mM, then decreased when concentration of $CaCl_2$ increased to 1 mM. The average zeta potential of CeO_2 NPs was less than 20 mV and close to 0 mV, which indicates the aggregation of CeO_2 NPs in the presence of HA and $CaCl_2$ at pH 8.2. The Pearson's correlation coefficients for the ξ potential values of CeO_2 NPs and time at pH 8.2 in the presence of HA in concentration of NaCl 0, 0.1, and 1 mM, $CaCl_2$ 0.1 and 1 mM are 0.01, −0.66, −0.35, −0.17, and −0.88, respectively.

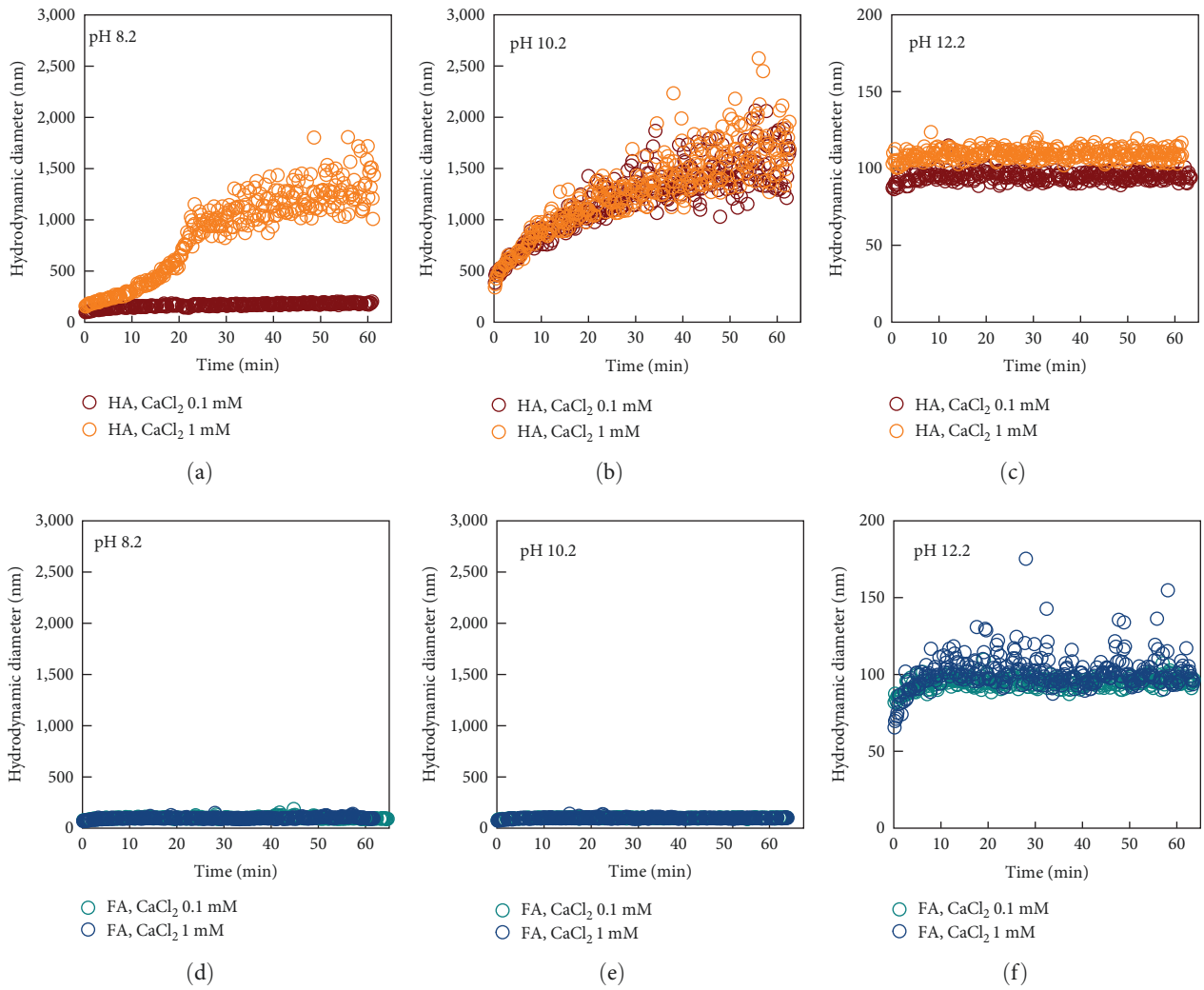

FIGURE 10: Hydrodynamic diameter measurements of CeO_2 NPs in the presence of HA (5 mg/L) or FA (0.14 mg/L) as a function of time, and $CaCl_2$ concentration ranging from 0 to 1 mM at pH 8.2, pH 10.2, and pH 12.2: (a) HA, $CaCl_2$, and pH 8.2; (b) HA, $CaCl_2$, and pH 10.2; (c) HA, $CaCl_2$, and pH 12.2; (d) FA, $CaCl_2$, and pH 8.2; (e) FA, $CaCl_2$, and pH 10.2; and (f) FA, $CaCl_2$, and pH 12.2.

However, the other parameters did not show the same prediction as zeta potential measurements.

At pH < pH_{PZC}, in the presence of HA, the average hydrodynamic diameter of CeO_2 NPs was smaller at 0.1 mM of NaCl/$CaCl_2$ than at both 0 and 1 mM of NaCl/$CaCl_2$ (Figures 9(a) and 10(a)). For instance, at ~1 hr, the hydrodynamic diameter of CeO_2 NPs at 1 mM $CaCl_2$ (1,397.18 ± 209.50 nm) was 649.24% greater than at 0.1 mM (186.48 ± 8.47 nm) (Table S4). At ~1 hr, the average hydrodynamic diameter in the presence of HA was larger than or close to it in the absence of HA. For instance, at ~1 hr, the hydrodynamic diameter of CeO_2 NPs at 0.1 mM NaCl in the presence of HA (183.78 ± 7.76 nm) was 65.05% greater than in the absence of HA (111.35 ± 2.83 nm). The particle size distribution of CeO_2 NPs during the first 100 s and at ~1 hr at pH value of 8.2 and in the presence of monovalent NaCl or divalent $CaCl_2$ salts as well as SRHA, all at various concentrations, is presented in Figures S4(a), S4(b), S4(g), and S4(h).

First k_{11} decreased then increased when the electrolyte concentration increased from 0 to 1 mM. It was smaller at 0.1 and 1 mM NaCl/$CaCl_2$ than at 0 mM of NaCl/$CaCl_2$ (Table 2). In the presence of HA, at 0.1 mM of salt, k_{11} in the presence of NaCl was smaller than in the presence of $CaCl_2$. In the presence of HA, at 1 mM of salt, k_{11} in the presence of NaCl was greater than in the presence of $CaCl_2$.

No energy barrier was found at 1 mM of NaCl/$CaCl_2$ in the presence of HA (Figures 12(a) and 12(d)). The values of energy barriers were 4.23, 2.83, and 2.96 kJ at 0 mM of NaCl, 0.1 mM of NaCl, and 0.1 mM of $CaCl_2$, respectively (Figures 12(a) and 12(d)). This finding indicates that at pH < pH_{PZC}, CeO_2 NPs are unstable at 1 mM of NaCl/$CaCl_2$.

3.4.2. Uncharged CeO_2 NPs in the Presence of HA (pH = 10.2 = pH_{PZC}). The aggregation profiles and average zeta potentials of CeO_2 NPs at pH value of 10.2 and in the presence of monovalent NaCl or divalent $CaCl_2$ salts as well as SRHA, all at various concentrations, are presented in Figures 9(b)

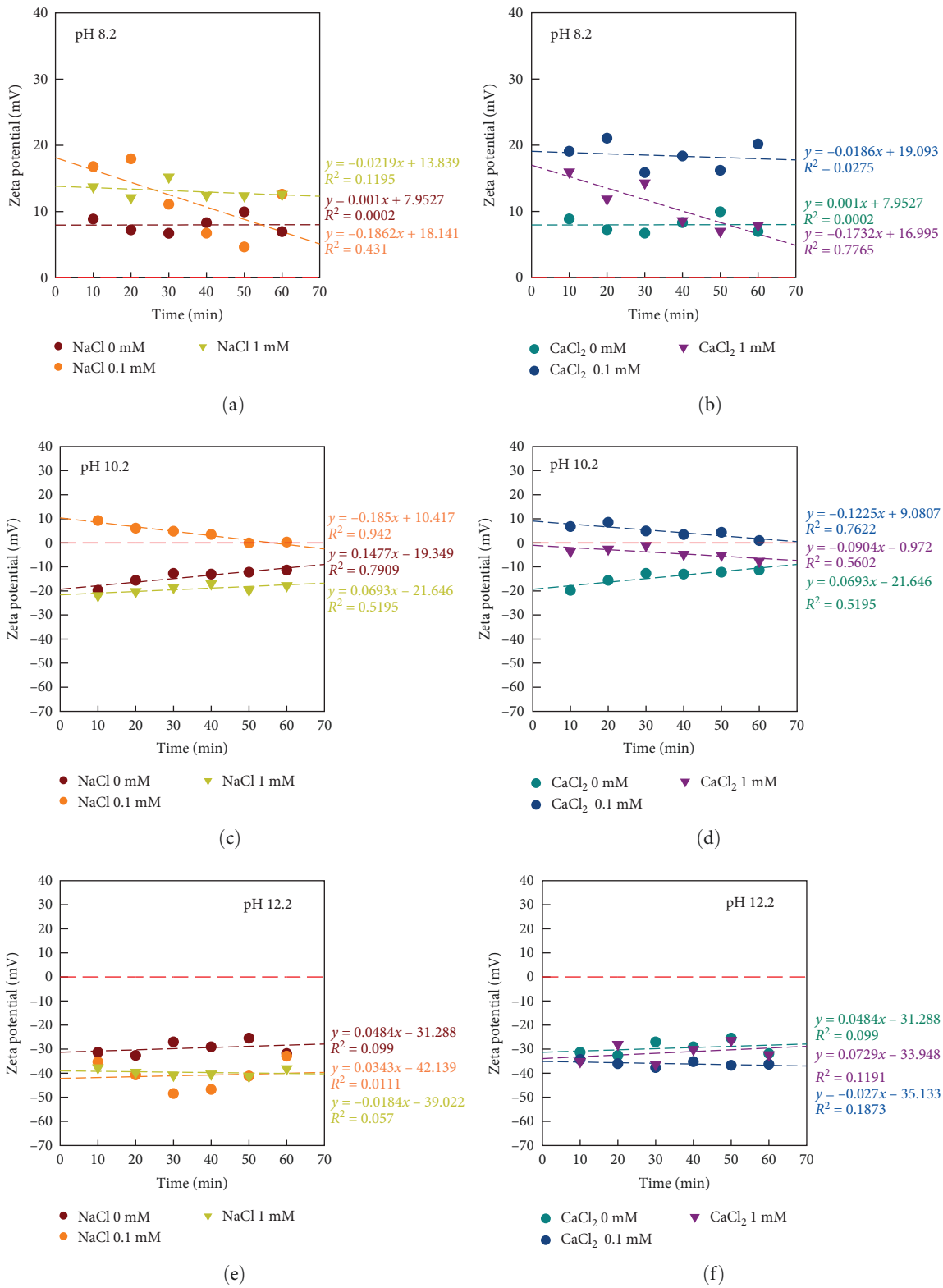

FIGURE 11: Zeta potential of CeO_2 NPs as a function of time in varying concentrations of NaCl or $CaCl_2$ in the presence of HA at pH 8.2, pH 10.2, and pH 12.2: (a) HA, NaCl, and pH 8.2; (b) HA, $CaCl_2$, and pH 8.2; (c) HA, NaCl, and pH 10.2; (d) HA, $CaCl_2$, and pH 10.2; (e) HA, NaCl, and pH 12.2; and (f) HA, $CaCl_2$, and pH 12.2.

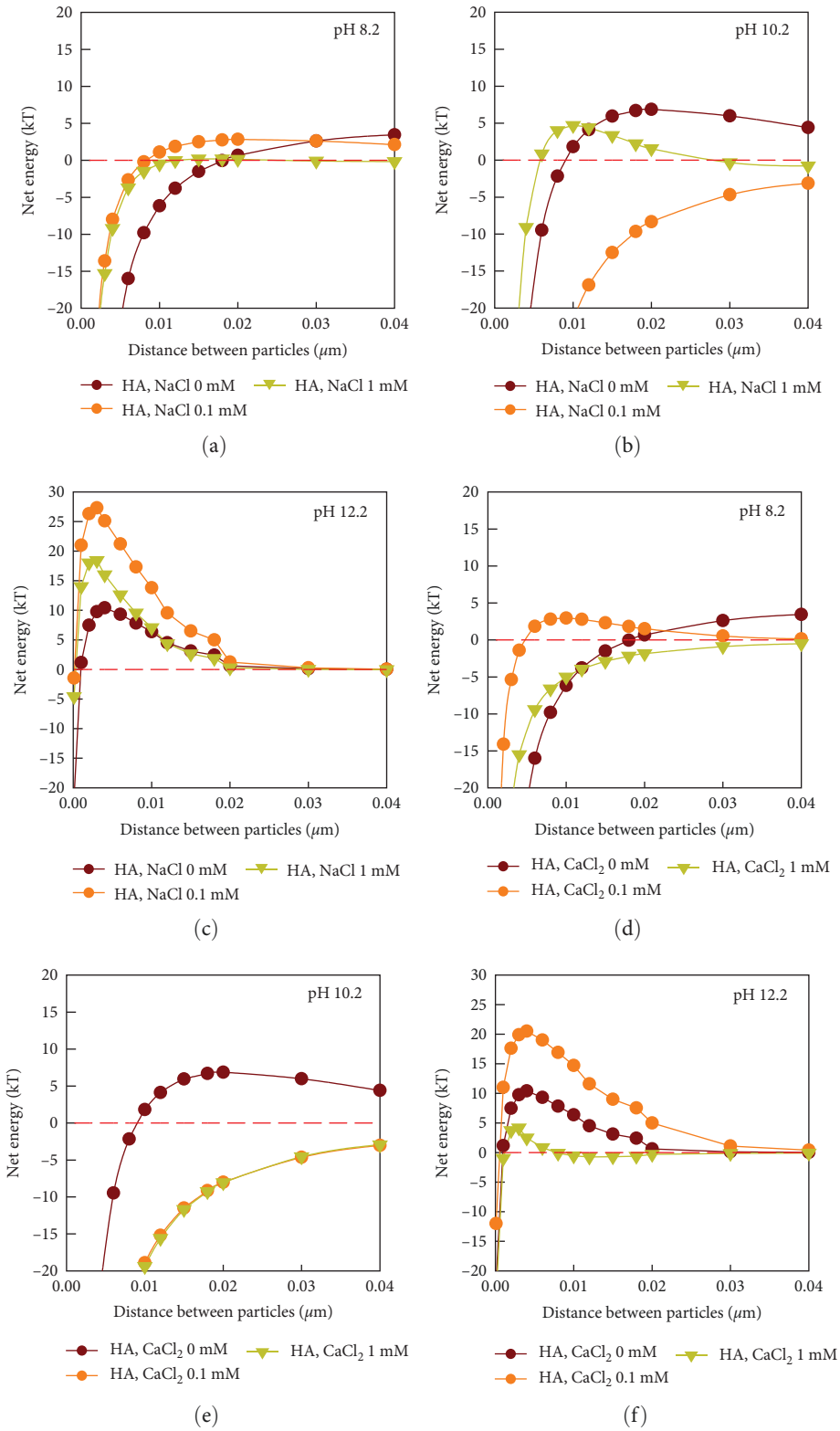

Figure 12: Net energy versus interparticle distance according to DLVO theory, showing the influence of HA (5 mg/L) and representative monovalent electrolyte NaCl or divalent electrolyte $CaCl_2$ concentrations varying from 0 to 1 mM at pH 8.2, pH 10.2, and pH 12.2, for CeO_2 NPs suspended in aqueous systems: (a) HA, NaCl, and pH 8.2; (b) HA, NaCl, and pH 10.2; (c) HA, NaCl, and pH 12.2; (d) HA, $CaCl_2$, and pH 8.2; (e) HA, $CaCl_2$, and pH 10.2; and (f) HA, $CaCl_2$, and 12.2. Calculation of DLVO theory includes the contributions of the van der Waals and electric double layer (EDL) interactions. The net energy (Net) shown is the sum of EDL repulsion and van der Waals attraction between two approaching particles.

and 10(b) and Figures 11(c) and 11(d), respectively. At pH 10.2 ($pH = pH_{PZC}$), the absolute average zeta potential of CeO_2 NPs varied about 0 mV and was less than 22 mV (Figures 11(c) and 11(d) and Table S2). The Pearson's correlation coefficients for the ξ potential values of CeO_2 NPs and time at pH 10.2 in the presence of HA in concentration of NaCl 0, 0.1, and 1 mM, $CaCl_2$ 0.1 and 1 mM are 0.89, −0.97, 0.72, −0.87, and −0.75, respectively. CeO_2 NPs were unstable in the presence of HA at $pH = pH_{PZC}$. This conclusion can also be predicted by the results of hydrodynamic diameter, k_{11}, and size distribution. The average hydrodynamic diameter of CeO_2 NPs grew at high rates and reached the micron level in the presence of HA after approximately 1 hr of incubation (Figures 9(b) and 10(b)). For example, in the presence of HA, the hydrodynamic diameter of CeO_2 NPs at 0.1 mM $CaCl_2$ increased by 236.61% at ∼1 hr (1,584.86 ± 223.48 nm) when compared to the hydrodynamic diameter during the first 100 s (470.83 ± 39.34 nm) (Table S4). The particle size distribution of CeO_2 NPs during the first 100 s and at ∼1 hr at pH value of 10.2 and in the presence of monovalent NaCl or divalent $CaCl_2$ salts as well as SRHA, all at various concentrations, is presented in Figures S4(c), S4(d), S4(i), and S4(j).

The k_{11} was in the range of 0.37–0.54 nm/s under all concentrations of NaCl/$CaCl_2$ in the presence of HA (Table 2).

No energy barrier was found at 0.1 mM of NaCl and at 0.1 and 1 mM of $CaCl_2$ (Figures 12(b) and 12(e)). The values of energy barriers were 6.87 and 4.70 kJ at 0 and 1 mM of NaCl (Figure 12(b)). This result indicates that at $pH = pH_{PZC}$, CeO_2 NPs are unstable in the presence of HA at 0.1 mM of NaCl, and at 0.1 and 1 mM of $CaCl_2$. This prediction is different from the prediction from the results of the other parameters above.

3.4.3. Negatively Charged CeO_2 NPs in the Presence of HA ($pH = 12.2 > pH_{PZC}$). The aggregation profiles and average zeta potentials of CeO_2 NPs at pH value of 12.2 and in the presence of monovalent NaCl or divalent $CaCl_2$ salts as well as SRHA, all at various concentrations, are presented in Figures 9(c) and 10(c) and Figures 11(e) and 11(f), respectively. At pH 12.2 ($pH > pH_{PZC}$), the average zeta potential of CeO_2 NPs was less than −30 mV during the 1 hr incubation in the presence of HA and NaCl/$CaCl_2$ (Figures 11(e) and 11(f) and Table S2), which indicates that CeO_2 NPs are stable in the presence of HA at $pH > pH_{PZC}$. The Pearson's correlation coefficients for the ξ potential values of CeO_2 NPs and time at pH 12.2 in the presence of HA in concentration of NaCl 0, 0.1, and 1 mM, $CaCl_2$ 0.1 and 1 mM are 0.31, 0.11, −0.24, −0.43, and 0.35, respectively.

The growth of hydrodynamic diameter of CeO_2 NPs was slow for all suspensions in the presence of HA over 1 hr (Figures 9(c) and 10(c)). At ∼1 hr, the average hydrodynamic diameter of CeO_2 NPs was less than 120 nm. For example, in the presence of HA, the hydrodynamic diameter of CeO_2 NPs at 1 mM NaCl increased only by 20.74% at ∼1 hr (93.86 ± 1.91 nm) when compared to the hydrodynamic diameter during the first 100 s (77.74 ± 2.31 nm) (Table S4). This finding also indicates the stability of CeO_2 NPs in the presence of HA at $pH > pH_{PZC}$ with the same prediction obtained from the other parameters. The particle size distribution of CeO_2 NPs during the first 100 s and at ∼1 hr at pH value of 12.2 and in the presence of monovalent NaCl or divalent $CaCl_2$ salts as well as SRHA, all at various concentrations is presented in Figures S4(e), S4(f), S4(k), and S4(l). The k_{11} was less than 0.02 nm/s at pH 12.2 for all suspensions in the presence of HA (Table 2). The net energy barriers were 10.4, 27.3, and 18.4 kJ, at 0, 0.1, and 1 mM of NaCl, respectively (Figure 12(c)). The net energy barriers were 20.5 and 4.16 at 0.1 and 1 mM of $CaCl_2$ (Figure 12(f)).

3.5. Impact of pH and FA on Stability of CeO_2 NPs. The effects of FA and cation (Na^+ and Ca^{2+}) concentrations on CeO_2 NPs stability in three pH domains representing the three electrostatic states—$pH = 8.2 < pH_{PZC}$, $pH = 10.2 = pH_{PZC}$, and $pH = 12.2 > pH_{PZC}$—were examined by measuring the surface charge and size of nanoparticles using ELS and DLS methods.

3.5.1. Positively Charged CeO_2 NPs in the Presence of FA ($pH = 8.2 < pH_{PZC}$). The aggregation profiles and average zeta potentials of CeO_2 NPs at pH value of 8.2 and in the presence of monovalent NaCl or divalent $CaCl_2$ salts as well as SRFA, all at various concentrations, are presented in Figures 9(d) and 10(d) and Figures 13(a) and 13(b), respectively. At $pH < pH_{PZC}$, in the presence of FA, the average zeta potential of CeO_2 NPs was less than −35 mV at 0, 0.1, and 1 mM of NaCl and at 0.1 mM of $CaCl_2$ (Figures 13(a) and 13(b) and Table S2). However, the average zeta potential of CeO_2 NPs ranged from −23 to −26 mV at 1 mM of $CaCl_2$. The Pearson's correlation coefficients for the ξ potential values of CeO_2 NPs and time at pH 8.2 in the presence of FA in concentration of NaCl 0, 0.1, and 1 mM, $CaCl_2$ 0.1 and 1 mM are −0.58, −0.21, −0.11, −0.67, and 0.56, respectively.

At ∼1 hr, the average hydrodynamic diameter of CeO_2 NPs in the presence of FA was less than 110 nm (Figures 9(d) and 10(d)). For example, in the presence of FA, the hydrodynamic diameter of CeO_2 NPs at 0.1 mM NaCl only increased by 9.12% at ∼1 hr (101.87 ± 3.36 nm) when compared to the hydrodynamic diameter during the first 100 s (93.36 ± 1.95 nm) (Table S5). This result indicates that FA stabilizes CeO_2 NPs at $pH < pH_{PZC}$. The same prediction is obtainable from the results of size distribution (Figure S5). The particle size distribution of CeO_2 NPs during the first 100 s and at ∼1 hr at pH value of 8.2 and in the presence of monovalent NaCl or divalent $CaCl_2$ salts as well as SRFA, all at various concentrations, is presented in Figures S5(a), S5(b), S5(g), and S5(h). Thus k_{11} was less than 0.02 nm/s at pH 8.2 for all suspensions in the presence of FA (Table 2).

However, at 1 mM of $CaCl_2$, the result of the net energy barrier was different from the other parameters in the presence of FA (Figures 14(a) and 14(d)). Here, energy barriers existed at all salt concentrations, except at that level (Figures 14(a) and 14(d)).

3.5.2. Uncharged CeO_2 NPs in the Presence of FA ($pH = 10.2 = pH_{PZC}$). The aggregation profiles and average zeta potentials of CeO_2 NPs at pH value of 10.2 and in the presence of

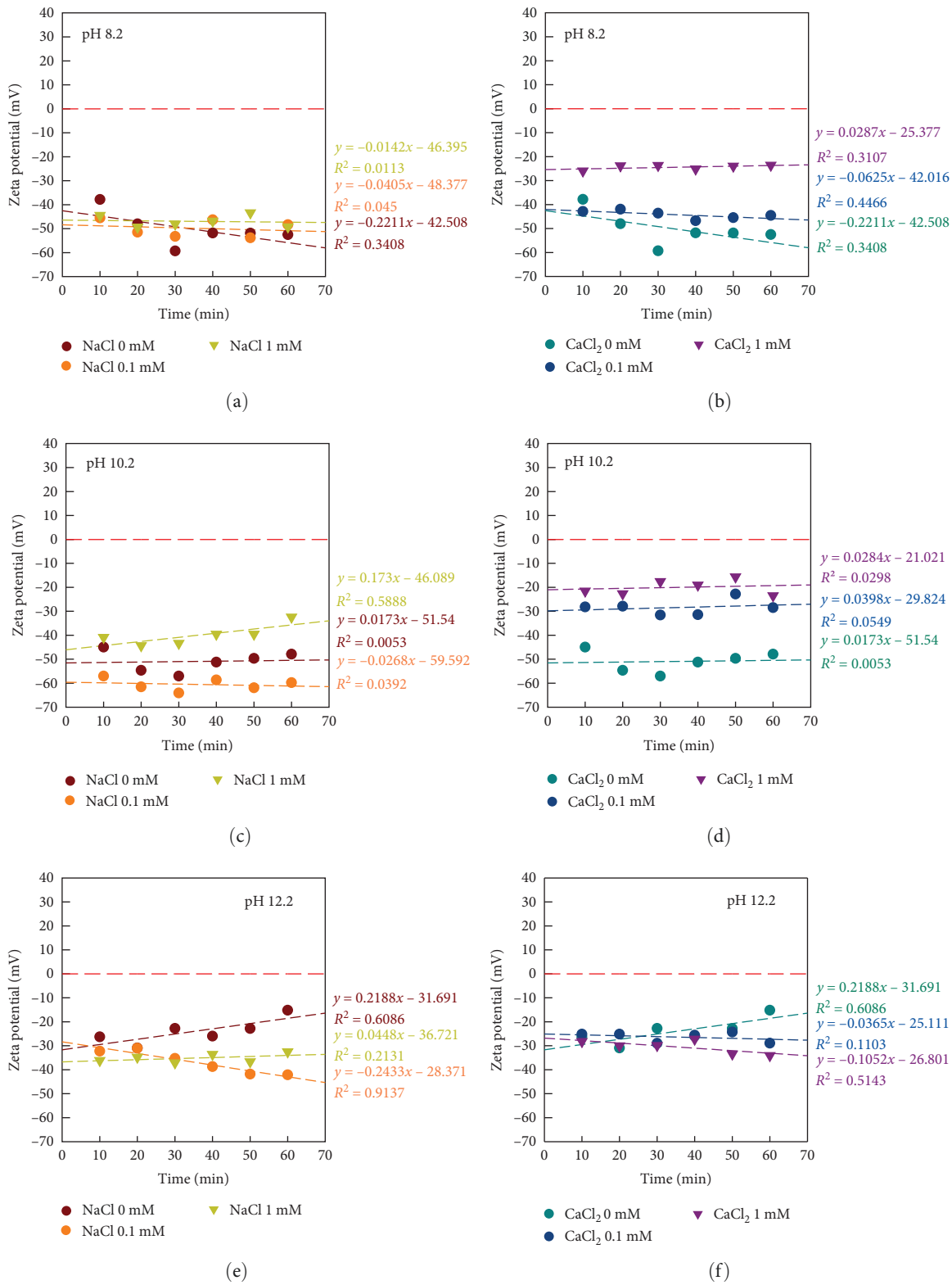

FIGURE 13: Zeta potential of CeO_2 NPs as a function of time in varying concentrations of NaCl or $CaCl_2$ in the presence of FA at pH 8.2, pH 10.2, and pH 12.2: (a) FA, NaCl, and pH 8.2; (b) FA, $CaCl_2$, and pH 8.2; (c) FA, NaCl, and pH 10.2; (d) FA, $CaCl_2$, and pH 10.2; (e) FA, NaCl, and pH 12.2; and (f) FA, $CaCl_2$, and pH 12.2.

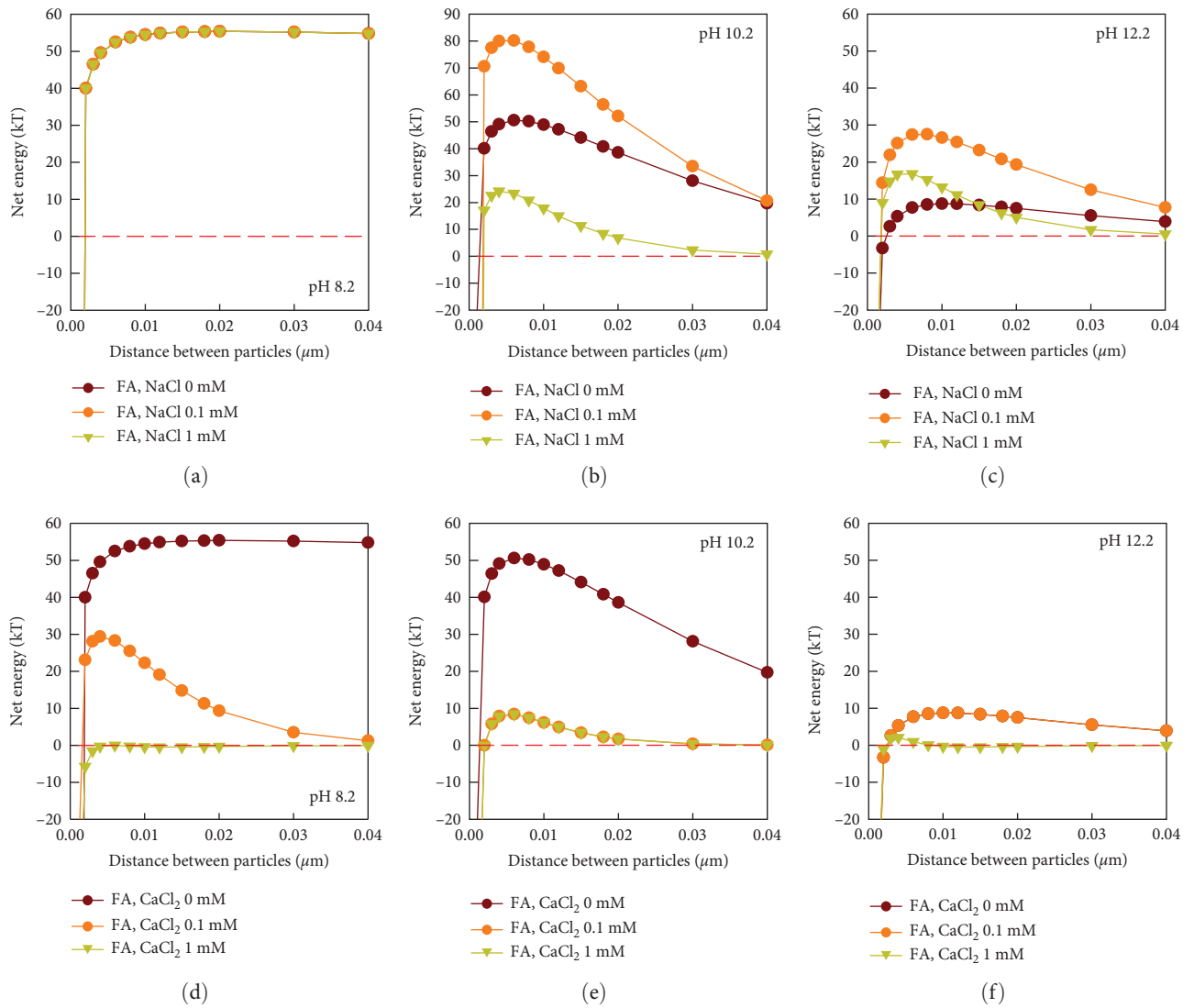

FIGURE 14: Net energy versus interparticle distance according to DLVO theory, showing the influence of FA (0.14 mg/L) and representative monovalent electrolyte NaCl or divalent electrolyte $CaCl_2$ concentrations varying from 0 to 1 mM at pH 8.2, pH 10.2, and pH 12.2, for CeO_2 NPs suspended in aqueous systems: (a) FA, NaCl, and pH 8.2; (b) FA, NaCl, and pH 10.2; (c) FA, NaCl, and pH 12.2; (d) FA, $CaCl_2$, and pH 8.2; (e) FA, $CaCl_2$, and pH 10.2; and (f) FA, $CaCl_2$, and 12.2. Calculation of DLVO theory includes the contributions of the van der Waals and electric double layer (EDL) interactions. The net energy (Net) shown is the sum of EDL repulsion and van der Waals attraction between two approaching particles.

monovalent NaCl or divalent $CaCl_2$ salts as well as SRFA, all at various concentrations, are presented in Figures 9(e) and 10(e) and Figures 13(c) and 13(d), respectively. At $pH = pH_{PZC}$, the average zeta potential of CeO_2 NPs was less than −30 mV in the presence of FA and NaCl (Figures 13(c) and 13(d) and Table S2). The average zeta potential of CeO_2 NPs was −15 to −32 mV in the presence of FA and $CaCl_2$. The Pearson's correlation coefficients for the ξ potential values of CeO_2 NPs and time at pH 10.2 in the presence of FA in concentration of NaCl 0, 0.1, and 1 mM, $CaCl_2$ 0.1 and 1 mM are 0.07, −0.20, 0.77, 0.23, and 0.17, respectively.

The results of hydrodynamic diameter, k_{11}, and size distribution indicated the stability of CeO_2 NPs in the presence of FA at pH 10.2. At ∼1 hr, the average hydrodynamic diameter of CeO_2 NPs in the presence of FA was less than 105 nm (Figures 9(e) and 10(e)). For example, in the presence of FA, the hydrodynamic diameter of CeO_2 NPs at 1 mM $CaCl_2$ increased only by 25.28% at ∼1 hr (97.02 ± 2.96 nm) when compared to the hydrodynamic diameter during the first 100 s (77.44 ± 4.25 nm) (Table S5). The particle size distribution of CeO_2 NPs during the first 100 s and at ∼1 hr at pH value of 10.2 and in the presence of monovalent NaCl or divalent $CaCl_2$ salts as well as SRFA, all at various concentrations, is presented in Figures S5(c), S5(d), S5(i), and S5(j). The k_{11} was less than 0.02 nm/s at pH 10.2 for all suspensions in the presence of FA (Table 2).

However, at pH 10.2, the net energy barrier existed in the presence of FA and NaCl/$CaCl_2$, except that the net energy barrier was 0 kT at 1 mM $CaCl_2$ (Figures 14(b) and 14(e)).

This finding indicates that CeO_2 NPs are not stable at 1 mM of $CaCl_2$.

3.5.3. Negatively Charged CeO_2 NPs in the Presence of FA ($pH = 12.2 > pH_{PZC}$). The aggregation profiles and average zeta potentials of CeO_2 NPs at pH value of 10.2 and in the presence of monovalent NaCl or divalent $CaCl_2$ salts as well as SRFA, all at various concentrations, are presented in Figures 9(f) and 10(f) and Figures 13(e) and 13(f), respectively. At pH 12.2 ($pH > pH_{PZC}$), at 0–1 hr, the average zeta potential varied from −24 to −38 mV for all suspensions in the presence of FA (Figures 13(e) and 13(f) and Table S2), a finding that shows the stability of CeO_2 NPs at pH 12.2. The Pearson's correlation coefficients for the ξ potential values of CeO_2 NPs and time at pH 12.2 in the presence of FA in concentration of NaCl 0, 0.1, and 1 mM, $CaCl_2$ 0.1 and 1 mM are 0.78, −0.96, 0.46, −0.33, and −0.72, respectively. The same prediction is obtainable from results of all the parameters below as the result of zeta potential measurements.

The average hydrodynamic diameter of the CeO_2 NPs grew at low rates in the presence of FA, and the average hydrodynamic diameter was less than 120 nm (Figures 9(f) and 10(f)). For example, in the presence of FA, the hydrodynamic diameter of the CeO_2 NPs at 1 mM NaCl only increased by 14.36% at ∼1 hr (94.35 ± 3.49 nm) when compared to the hydrodynamic diameter during the first 100 s (82.50 ± 1.77 nm) (Table S5). The particle size distribution of CeO_2 NPs during the first 100 s and at ∼1 hr at pH value of 10.2 and in the presence of monovalent NaCl or divalent $CaCl_2$ salts as well as SRFA, all at various concentrations, is presented in Figures S5(e), S5(f), S5(k), and S5(l). The k_{11} was less than 0.02 nm/s at pH 12.2 for all suspensions in the presence of FA (Table 2). In the presence of FA, net energy barriers existed under all electrolyte concentrations at pH 12.2 (Figures 14(c) and 14(f)).

4. Discussion

The stability of NPs derives from their ability to remain unchanged over time under certain conditions. The importance of studying the stability of the CeO_2 NPs is that their stability affects their transport, retention, bioavailability, and toxicity while posing potential risks to the environment and human health.

4.1. Effect of pH on the Stability of CeO_2 NPs (Homoaggregation). The pH is one of the water chemistry parameters that affect NPs aggregation by altering the charge on the surface of NPs [69]. At both low and high pH levels, the aggregation was extremely constrained but was enhanced as the pH approached pH_{PZC} [92].

Homoaggregation, a term which refers to the aggregation of two similar CeO_2 NPs [93], was affected by the changing pH conditions presented in this study. The stability of CeO_2 NPs in aqueous systems differed at various pH domains. Although the CeO_2 NPs were stable at $pH < pH_{PZC}$ (except for 1 mM of NaCl/$CaCl_2$) and at $pH > pH_{PZC}$ (except for 0.5 mM $CaCl_2$), the aggregation was enhanced at $pH = pH_{PZC}$.

The phenomena and explanations of the aggregation and stability of CeO_2 NPs in three pH domains ($pH < pH_{PZC}$, $pH = pH_{PZC}$, and $pH > pH_{PZC}$) in our research are summarized below.

At $pH < pH_{PZC}$, the average hydrodynamic diameter of CeO_2 NPs at 1 mM of salt during the first 100 s (approximately 165 nm) was much lower than that at ∼1 hr (above 1,000 nm) (Figures 4(b) and 7(b)). The CeO_2 NPs were stable at either no or low concentration of electrolytes (<1 mM) and were unstable at higher concentration (1 mM) of electrolytes. This conclusion was demonstrated by the results of DLVO theory analysis on the net energy interaction among CeO_2 NPs: the repulsive energy barriers were found at 0–0.5 mM NaCl/$CaCl_2$ but not shown at 1 mM NaCl/$CaCl_2$ (Figures 6(a) and 6(d)).

One possible explanation is that at $pH < pH_{PZC}$, surface protonation occurs when the protons adsorb to the hydration layer capped on CeO_2 NPs, thus preventing the further aggregation of CeO_2 NPs. The occurrence of suspensions in either the absence of electrolyte or in the presence of low electrolyte results in a dominance of the repulsive interaction from the large distance separations between CeO_2 NPs. However, the increase in electrolyte concentration led to the compression of the double layer of CeO_2 NPs and reduced the stability of CeO_2 NPs. The strongly positively charged surface of CeO_2 NPs at $pH < pH_{PZC}$ resulted in the predominated role of electrostatic repulsion over attraction; thus the stability of CeO_2 NPs was enhanced. Similarly, due to the same mechanism above, the low pH enhanced the CeO_2 NP mobility, a result that is attributable to the increased stability of the CeO_2 NPs [40]. The similar influence of electrolyte on the stability of CeO_2 NPs was also noted in that the CeO_2 NPs were stable at low NaCl concentrations (<10 mM) and unstable at higher NaCl concentrations (>10 mM). Further, the positive zeta potentials determined for three different synthesized CeO_2 NPs had isoelectric points at pH 5.8, 7.6, and 6.5 [52]. The uncoated CeO_2 NPs exhibited positive zeta potentials at pH less than its pH_{PZC} (pH 6.8 ± 0.1) [44]. In addition, at pH 4.5 (i.e., $pH < pH_{PZC}$), TiO_2 NPs nanoaggregate size was substantially greater, and the size distribution became broader at a higher IS (0.165 M) in the presence of NaCl/$CaCl_2$ [79]. However, no obvious aggregation was evident at a lower IS (0.0045 M).

At a $pH = pH_{PZC}$, the largest aggregation sizes were obtained. This finding was in correlation to the close-to-zero average zeta potentials (Table S2), the large values of the average hydrodynamic diameter of CeO_2 NPs (1,300–3,600 nm) at ∼1 hr (Figures 4(c) and 4(d), Figures 7(c) and 7(d), and Table S3), and the lack of a repulsive energy barrier (0 kT) (Figures 6(b) and 6(e)). This outcome suggests that at $pH = pH_{PZC}$, the electrostatic attraction is predominant over the repulsion, and destabilization behavior exists in the suspensions. Similarly, a pH level approximate to the pH_{PZC} (pH 6.5) increased the protons that then reacted with the functional groups (e.g., carboxyl groups) with a negative surface charge, thus reducing the CeO_2 NP surface charges to the benefit of the aggregation [40]. However, in their

study, Oriekhova and Stoll [44] reported that the average hydrodynamic diameter of CeO_2 NPs was near 2,000 nm at $pH = pH_{PZC}$. Quik et al. [63] also noted a discrepancy in pH_{PZC} that was equal to pH 8 in 10 mg/L CeO_2 NP samples. The differences in these studies of the pH_{PZC} of CeO_2 NP are perhaps due to the purchasing of nanoparticles created with various synthesizing techniques, and a difference in the concentrations, solution/suspension conditions, and mediums used in the experiments. Similarly, the pH_{PZC} values for the TiO_2 NPs also varied due to the technique used and constituents introduced during the synthesis [94]. In addition, the enhanced aggregation behavior of other types of NPs also occurred when the surface charge of the NPs was near the pH_{PZC}. When the pH reached the range of 5–8, large TiO_2 nanoaggregates formed, suggesting neutralization as the primary catalyst in nanoaggregate formation [95].

The enhanced aggregation behavior at $pH = pH_{PZC}$ in our research is explained by the occurrence of the surface charge neutralization of CeO_2 NPs from the interaction of hydroxyl ions with the CeO_2 NP surfaces. The condensation reaction, which is the inverse of hydrolysis, is expressed below [96]:

$$\text{M-OH}_2^{+} + \text{OH}^{-} = \text{M-OH} + \text{H}_2\text{O}. \quad (2)$$

with M-OH_2^{+} indicating the products after the interactions among CeO_2 NPs—water interface and H^+.

The hydrolysis reaction mechanism was used to demonstrate the impact of pH on aggregation of TiO_2 NPs by adding $FeCl_3$ [97] and on aggregation of iron oxide nanoparticles [98]. The hydrolysis complex structure of C_{60} NPs was also considered as the reason for the initial decrease in pH caused by the decrease of the absolute zeta potential [99]. In addition, at $pH = pH_{PZC}$, the maximum aggregation sizes were observed for TiO_2, titanate nanotubes, and titanate nanotubes-TiO_2 (800–1,300 nm) [100] and for ZnO NPs (1,802 nm) [101]. The destabilization was also present for ZnO NPs at pH 9, which was close to pH_{PZC} (9.2) [102].

At $pH > pH_{PZC}$, the surface deprotonation continues processing the large amount of OH^- interacting with surface of CeO_2 NPs. The large amount of OH^- adsorbed on the CeO_2 NP surfaces in turn yields strongly negatively charged and stable CeO_2 NPs (close to or less than −30 mM) at pH 12.2 (Table S2). Small CeO_2 nanoaggregates were present after an hour incubation, which was less than 190 nm, as shown in Figures 4(e) and 4(f) and Figures 7(e) and 7(f). Similarly, the homoaggregation of CeO_2 NPs at pH 11, which was larger than its pH_{PZC}, was enhanced with the increase of NaCl and $CaCl_2$ until they reached their CCC values [52]. In addition, the negatively charged TiO_2 NPs (with an approximate zeta potential of −55 mV) were stable (with an average hydrodynamic diameter near 120 nm) at a high pH [95]. In correspondence to the small CeO_2 nanoaggregates, we obtained small aggregate rates (<0.02 nm/s) in our study. A low aggregation rate (i.e., close to 0 nm/min) was also obtained for negatively charged TiO_2 NPs (with a zeta potential of −38.7 mV) at $pH > pH_{PZC}$ [103]. At pH 11–12 ($pH > pH_{PZC} = 7.8$), small nanoaggregates (<50 nm) formed at a low concentrations of iron oxide NPs (<50 mg/L) [104]. Moreover, at pH 9 ($pH > pH_{PZC}$), the Fe_3O_4 NPs were more unstable in the presence of divalent cations (e.g., Ca^{2+}) than in the presence of monovalent cations (Na^+) [105]. The size of Ag NPs was below 100 nm—at pH 8 because of the negative zeta potential from the negatively charged OH^- [106].

4.2. Effect of HA and FA on the Stability of CeO_2 NPs (Heteroaggregation). Although the HA stabilized CeO_2 NPs under $pH > pH_{PZC}$, the aggregation was enhanced at $pH = pH_{PZC}$ and in the presence of 0 and 1 mM of NaCl/$CaCl_2$ at $pH < pH_{PZC}$. Further, the FA stabilized CeO_2 NPs at all three pH levels ($pH >, =$, and $< pH_{PZC}$) and under all electrolyte concentrations (0–1 mM of NaCl or $CaCl_2$).

Heteroaggregation is a phenomenon that is characterized by dissimilar particle aggregation [93], the mechanisms of which between SRHA or SRFA and CeO_2 NPs differ from the mechanisms of homoaggregation between CeO_2 NPs. The adsorbed NOM on the NP surface was not only found to increase electrostatic repulsive forces between NPs but also cause steric forces, thus reducing NP aggregation [107–109]. In addition, the NOM sorption on the particles can facilitate the cation bridging and enhance both NOM and particle heteroaggregation (e.g., graphene oxide) [110]. Moreover, NOM can also neutralize the positive surface charge of NPs and enhance the aggregation [94]. Therefore, the complex nature of the heteroaggregation state and stability of CeO_2 NPs in the presence of HA or FA was also affected by both the pH and ionic composition and concentration.

4.2.1. Stable CeO_2 NPs with HA. The CeO_2 NPs under study here exhibited stability after a 1 hr incubation period in terms of the zeta potential (with the absolute value either near, or larger than, 30 mV). Further, the average hydrodynamic diameter was less than 120 nm for CeO_2 NPs in the presence of HA at all NaCl/$CaCl_2$ concentrations (0–1 mM) at pH 12.2 (Figures 9(c) and 10(c) and Table S2). The dispersion of CeO_2 NPs by HA at $pH > pH_{PZC}$ may account for the electrosteric stabilization, which is caused by the steric repulsion between the complexes of CeO_2 NPs and negatively charged HA. This finding agrees with the studies involving the use of NOM and particularly HA in CeO_2 NP stabilization [47, 49] and other types of NPs [68, 69, 97, 111, 112]. Both the electrostatic and steric stabilization mechanisms were also determined as catalysts for enhancing the NP stabilization [101, 113–116]. Further, the low average hydrodynamic diameter (<1,000 nm) of CeO_2 NPs in the presence of NOM was present at a high pH and a low IS [49]. HA was an important catalyst in stabilizing the TiO_2 NPs and forming small-size nanoaggregates (of approximately 250 nm) in natural waters due to the effects of both the electrostatic and steric repulsion [69]. The TiO_2 NPs surface was covered by the HA molecules, and the aggregation was inhibited at a high pH [97]. We also found that the stability of CeO_2 NPs was higher in the presence of HA at $pH > pH_{PZC}$ than at other pHs in our study. At a $pH > pH_{PZC}$, the increase of HA (from 0 to 1 mg/L) decreased the zeta potentials from <−20 to −25.8 mV and −30 to −35.65 mV for both the

anatase and rutile TiO_2 NPs, with a 120 nm size at 1 mg/L HA, indicating that HA stabilized these TiO_2 NPs [94]. However, at pH < pH_{PZC}, the increase of HA (0–1 mg/L) neutralized the positively charged TiO_2 NPs, resulting in close to 0 mV zeta potentials (−4 mV for the anatase TiO_2 NPs and −9 mV for the rutile TiO_2 NPs) and unstable TiO_2 NPs. In another example, at basic pH (pH 8 and 10), Ag NPs were stable with a small hydrodynamic diameter (around 120 nm) in the presence of SRHA [117].

Inhibited aggregation was also in the presence of HA at 0.1 mM of salt (NaCl or $CaCl_2$) at pH 8.2 (Figures 9(a) and 10(a) and Table S2) due to the low k_{11} values of CeO_2 NPs (less than 0.05 nm/s). The stability of CeO_2 NPs is higher than predicted by the values of average zeta potential at pH < pH_{PZC}, a finding that indicates that steric stabilization inhibits the growth of CeO_2 nanoaggregates [17].

4.2.2. Unstable CeO_2 NPs with HA. Four concepts indicated the instability of the CeO_2 NPs in the presence of HA under 0 and 1 mM of salt (NaCl or $CaCl_2$) at pH 8.2 and in the presence of HA at all NaCl/$CaCl_2$ concentrations (0–1 mM) at pH 10.2. These are (i) an average hydrodynamic diameter larger than 1,500 nm (Figures 9(a) and 9(b) and Figures 10(a) and 10(b)); (ii) an absolute average zeta potential value less than 20 mV (Table S2); (iii) an aggregation rate larger than 0.35 nm/s (Table 2); and (iv) the values of repulsive energy barriers smaller than 7 kT (Figures 12(a), 12(b), 12(d), and 12(e)). A summary of the possible mechanisms and explanations for the unstable CeO_2 NPs at different pH and salt concentrations is below.

The predominance of protons that neutralize the CeO_2 NP surface charges may cause the CeO_2 NP instability in the presence of HA at all Na^+ or Ca^{2+} concentrations (0–1 mM) at pH = pH_{PZC}, though negatively charged HA exists in the systems. This instability also indicates the insufficiency of 5 mg/L HA in stabilizing the CeO_2 NPs (25 mg/L) at pH 10.2.

HA adsorption on the partial surface of CeO_2 NPs may be the cause of CeO_2 NP destabilization at pH < pH_{PZC} in the presence of HA and the absence of salt, thus increasing the CeO_2 NP hydrophobicity while promoting aggregation, also stated by Ghosh et al. [68] and Chen et al. [94]. HA neutralized the positive charges on the CeO_2 NP surfaces at pH < pH_{PZC}, which decreased the repulsive forces between the NPs and increased aggregation. HA can also lead to charge neutralization and NP destabilization [118, 119]. Similar phenomena and mechanisms were also identified for magnetite NPs [120]. In their study, Hu et al. [120] determined that HA increased the magnetite NP aggregation under changing pH conditions. In the presence of low HA concentrations (2 and 3 mg/L), the aggregation was enhanced at low pHs. The enhanced aggregation of CeO_2 NPs at 1 mM NaCl, as compared to the 0.1 mM NaCl, is from the compression of EDLs caused by an increase in IS. Similarly, Quik et al. [63] found that the steric repulsion of NOM had little effect upon the stability of the CeO_2 NPs. The aggregation of CeO_2 NPs was enhanced (i.e., the average hydrodynamic diameter increased from 173 to 253 nm) with the increase of electrolytes content in NOMs [63]. Also, a study of transport and deposition of SRHA-formed Ag NPs noted a marked instability of Ag NPs at a low acidic pH and a high IS [117]. In their study of CeO_2 NP destabilization, Li and Chen [47] noted an enhanced CeO_2 NP aggregation in the presence of HA, at a high $CaCl_2$ concentration of (80 mM) and a 5.7 pH (pH < pH_{PZC}). This type of CeO_2 NP aggregation is due to the bridging effect. In the bridge effect, interactions between HA and Ca^{2+} result in the formation of large HA aggregates via Ca^{2+} complexation which can bridge NPs and induce their aggregation [121]. In our study, we noted the enhanced aggregation in the presence of HA at 1 mM of Ca^{2+} at pH 8.2. Here the average zeta potential was approximately 10 mV (Table S2), the average hydrodynamic diameter was larger than 1,300 nm after a 1 hr incubation period (Figure 10(a)), and the slope of growth of CeO_2 NPs in the hydrodynamic diameter was larger than 0.10 nm/s (Table 2). Similarly, the bridging attraction between CeO_2 NPs induced by the aggregation of HA via Ca^{2+} was also found when the CeO_2 NPs were in the presence of HA and under high concentrations of Ca^{2+} [47]. The CeO_2 NPs were more unstable at a higher IS in the presence of NOM, and the CeO_2 nanoaggregates were larger than 1,000 nm [49]. Similar aggregation behaviors due to the inter-molecule bridging effect has been found among other types of NPs, such as C_{60} NPs [121] and Ag NPs [122]. In addition, NPs (e.g., Ag NPs or C_{60}) in the systems of SRHA or SRNOM were more unstable with high divalent cations than with monovalent cations [123, 124]. The bridging effect of NOM and Ca^{2+} increased the aggregation of other types of NPs, such as citrate-coated gold nanoparticles [125], iron oxide NPs [126], and other types of NPs [127]. In another example, the aggregation of silicon NPs was enhanced in the presence of SRHA and Ca^{2+} due to the bridging effect of SRHA with Ca^{2+} overweighing the compression of the EDL between NPs by Ca^{2+} [128].

4.2.3. Stable CeO_2 NPs with FA. In this research, the CeO_2 NPs were very stable in the presence of FA (0.14 mg/L) at all three pHs (8.2, 10.2, and 12.2) and under all electrolyte concentrations (0–1 mM of NaCl or $CaCl_2$) (Figures 9(d)–9(f) and Figures 10(d)–10(f)). This finding indicates that lower concentration of FA in our study can completely coat the surface of CeO_2 NPs and strongly stabilize CeO_2 NPs due to steric hindrance and increased electrostatic repulsion as indicated by the high absolute zeta potential values. Recent studies on the influence of FA upon the stability of CeO_2 NPs also noted the similar prevention of CeO_2 NP aggregation. Specifically, Oriekhova and Stoll [44] found that CeO_2 NPs were stable at pH 8 (the average hydrodynamic diameter < 210 nm) in the presence of 2 mg/L of FA. They also reported that the negative zeta potential and the small average hydrodynamic diameter (no larger than 220 nm) were due to the formation of CeO_2 NP–FA complexes, as indicated on SEM imagery [45]. Similar stable nanoaggregates were also present among other types of NPs. The increase of surface charge and formation of surface coating caused by FA was also evidenced in the study of cit-AgNPs, where adsorption of FA on cit-AgNPs led to electrosteric stabilization [89]. In the presence of FA and a high IS, the TiO_2 NPs

were stabilized [129]. Similarly, the FA adsorption to other types of NPs (e.g., TiO_2 NPs, C_{60} NPs, Ag NPs, iron oxide NPs) and stabilizing effects of FA on NPs were attributed to steric effects and compression of the diffusive layer of both NPs and FAs [89, 129, 130].

It is known that FA has a lower molecular weight (500–2,000 g/mol) than HA (1,000–10,000 g/mol) with HA in many cases deemed more effective than FA in stabilizing NPs [87, 115, 130–133]. However, in our research, CeO_2 NPs in the presence of FA (0.14 mg/L) exhibited a greater degree of stability than CeO_2 NPs in the presence of HA (5 mg/L) at all three alkaline pH levels. This phenomenon suggests that FA has stronger electrostatic interactions than HA at those alkaline pH levels. The reason may be that FA is more aromatic and thus has increased the phenolic groups ionization and low hydrogen interaction-forming open structures than HA in alkaline pH [134, 135].

5. Conclusion

Our research provides a framework for understanding colloid systems and interfaces stability of engineered nanoparticles, CeO_2 NPs, in aqueous environments. The authors conducted a series of experiments to elucidate the physical and chemical interaction mechanisms that govern the colloidal stability and aggregation kinetics of CeO_2 NPs under the influence of soil and water abiotic factors—pH, ionic composition (monovalent NaCl and divalent $CaCl_2$ salts), and SRHA and SRFA. Experimental results showed that the solution chemistry affected the colloidal stability and aggregation kinetics of CeO_2 NPs. As a first key finding, this research demonstrated the effects of pH and salt on colloid systems and interfaces stability of CeO_2 NPs. The zeta potential of CeO_2 NPs, with pH_{PZC} of 10.2, decreased (from positive to negative) with increasing solution pH. The diameter of CeO_2 NP aggregates was ~1,700 nm in the region of pH_{PZC}, and decreased with pH at $pH < pH_{PZC}$ or $pH > pH_{PZC}$ to ~100 nm, except at pHs 1, 13, and 14, where it reached ~1,500–2,250 nm. The impacts of Na^+ and Ca^{2+} cations and HA and FA on the levels and rates of aggregation were pH-dependent.

Additionally, in the presence of salts, CeO_2 NPs were stable at $pH < pH_{PZC}$ (except for 1 mM of $NaCl/CaCl_2$) and $pH > pH_{PZC}$ (except for 0.5 mM $CaCl_2$); however, the aggregation was enhanced at $pH = pH_{PZC}$, with a diameter of CeO_2 NPs in the ~1,300–3,600 nm range. Next, HA stabilized CeO_2 NPs under $pH > pH_{PZC}$; however, the aggregation was again enhanced at $pH = pH_{PZC}$ with a diameter of CeO_2 NPs in the ~1,500–1,900 nm range, and in the presence of 0 and 1 mM of $NaCl/CaCl_2$ at $pH < pH_{PZC}$. FA (0.14 mg/L) showed more efficiency in stabilizing the CeO_2 NPs than HA (5 mg/L) at three pH levels (8.2, 10.2, and 12.2) and under all different electrolyte concentrations (0–1 mM of NaCl or $CaCl_2$). The diameter of CeO_2 NPs in the presence of FA grew at low rates and was ~95–115 nm at all three pHs and under all different electrolyte concentrations.

The significant impact of the solution chemistry (i.e., pH, salts, HA, and FA) in which CeO_2 NPs were suspended is linked to the development of interfacial complexation in aqueous environments, this finding is the second key result of this research. Particularly, besides the EDL compression effect by Ca^{2+}, between CeO_2 NPs, the ion bridging effect between CeO_2 NPs in Ca^{2+}-HA systems was a key controlling mechanism of the stability of CeO_2 NPs. Furthermore, FA inhibited the aggregation of CeO_2 NPs by enhancing the energy barrier, therefore allowing CeO_2 NPs to remain stable at pH values of 8.2, 10.2, and 12.2, and with NaCl and $CaCl_2$ concentrations ranging from 0 to 1 mM.

The risk assessment for CeO_2 NPs contamination, according to their aggregation and stability state in surface water and in the subsurface soils and aquifers, is of great importance for future regulation and evaluation of CeO_2 NPs waste disposal and applications in products. In rivers and oceans that are abundant with HA or FA, CeO_2 NPs are likely to be suspended and freely transported from one aquatic region to another, posing risks for aquatic animals and human swimming in a CeO_2 NPs-contaminated water. However, under some specific conditions with different solution chemistries, CeO_2 NPs form aggregates, settle at the bottom of the water compartments, become sediment contaminants uptake by sediment-dwelling animals, and enter the food chains. Therefore, additional testing of the CeO_2 NPs aggregation behavior and stability and other possible interactions under different solution chemistry is required to develop a data collection bank for CeO_2 NPs for the accurate and precise analysis, interpretation, and prediction for environmental risk assessment and protection.

Data Availability

The datasets generated during and/or analyzed during the current study are available from the corresponding author upon reasonable request.

Disclosure

This article is based on a chapter from the Ph.D. dissertation titled "Stability and Toxicity of Cerium Oxide Nanoparticles in Water-Soil-Plant Systems" by Linlin Mu, Clemson University, Clemson, SC, United States (2019) [136].

Conflicts of Interest

The authors declare that they have no conflicts of interest.

Authors' Contributions

L.M. and C.J.G.D. contributed to conceptualization, data curation, and methodology. L.M., M.G., and C.J.G.D. contributed to formal analysis. L.M., P.C.B., and C.J.G.D. contributed to investigation. L.M. contributed to writing—original draft preparation. L.M., M.G., P.C.B., and C.J.G.D. contributed to writing—review and editing. C.J.G.D. contributed to funding acquisition.

Acknowledgments

We wish to convey our appreciation to Clemson University for supporting this work. Open access funding enabled and organized by Carolinas 2023.

Supplementary Materials

The supplementary materials contain additional information on the hydrodynamic diameter of CeO_2 NPs during the first 100 s and at ∼1 hr of around 1 hr measurements for each pH (1–14); the particle size distribution of CeO_2 NPs during the first 100 s and at ∼1 hr of around 1 hr measurements for each pH (1–14); the zeta potential of CeO_2 NPs under varying concentrations of NaCl/$CaCl_2$ in the absence/presence of HA/FA at three different pHs (8.2, 10.2, and 12.2) and different time intervals of around 1 hr measurements; the hydrodynamic diameter of CeO_2 NPs during the first 100 s and at ∼1 hr of around 1 hr measurements at three different pHs (8.2, 10.2, and 12.2) and each NaCl/$CaCl_2$ concentration; the particle size distribution of CeO_2 NPs during the first 100 s and at ∼1 hr of around 1 hr measurements in the presence of NaCl at three different pHs (8.2, 10.2, and 12.2); the particle size distribution of CeO_2 NPs during the first 100 s and at ∼1 hr of around 1 hr measurements in the presence of $CaCl_2$ at three different pHs (8.2, 10.2, and 12.2); the hydrodynamic diameter of CeO_2 NPs during the first 100 s and at ∼1 hr of around 1 hr measurements at three different pHs (8.2, 10.2, and 12.2) and each NaCl/$CaCl_2$ concentration in the presence of HA; the particle size distribution of CeO_2 NPs during the first 100 s and at ∼1 hr of around 1 hr measurements in the presence of HA, NaCl, and $CaCl_2$ at three different pHs (8.2, 10.2, and 12.2); the hydrodynamic diameter of CeO_2 NPs during the first 100 s and at ∼1 hr of around 1 hr measurements at three different pHs (8.2, 10.2, and 12.2) and each NaCl/$CaCl_2$ concentration in the presence of FA; and the particle size distribution of CeO_2 NPs during the first 100 s and at ∼1 hr of around 1 hr measurements in the presence of FA, NaCl, and $CaCl_2$ at three different pHs (8.2, 10.2, and 12.2). (*Supplementary Materials*)

References

[1] A. A. Keller, S. McFerran, A. Lazareva, and S. Suh, "Global life cycle releases of engineered nanomaterials," *Journal of Nanoparticle Research*, vol. 15, Article ID 1692, 2013.

[2] N. Z. Jankovic and D. L. Plata, "Engineered nanomaterials in the context of global element cycles," *Environmental Science-Nano*, vol. 6, no. 9, pp. 2697–2711, 2019.

[3] E. Bekyarova, P. Fornasiero, J. Kašpar, and M. Graziani, "CO oxidation on Pd/CeO_2-ZrO_2 catalysts," *Catalysis Today*, vol. 45, no. 1–4, pp. 179–183, 1998.

[4] K. Van Hoecke, J. T. K. Quik, J. Mankiewicz-Boczek et al., "Fate and effects of CeO_2 nanoparticles in aquatic ecotoxicity tests," *Environmental Science & Technology*, vol. 43, no. 12, pp. 4537–4546, 2009.

[5] K. Nakagawa, Y. Murata, M. Kishida, M. Adachi, M. Hiro, and K. Susa, "Formation and reaction activity of CeO_2 nanoparticles of cubic structure and various shaped CeO_2-TiO_2 composite nanostructures," *Materials Chemistry and Physics*, vol. 104, no. 1, pp. 30–39, 2007.

[6] T. Sato, T. Katakura, S. Yin, T. Fujimoto, and S. Yabe, "Synthesis and UV-shielding properties of calcia-doped ceria nanoparticles coated with amorphous silica," *Solid State Ionics*, vol. 172, no. 1–4, pp. 377–382, 2004.

[7] F. R. Cassee, E. C. van Balen, C. Singh et al., "Exposure, health and ecological effects review of engineered nanoscale cerium and cerium oxide associated with its use as a fuel additive," *Critical Reviews in Toxicology*, vol. 41, no. 3, pp. 213–229, 2011.

[8] A. C. Johnson and B. Park, "Predicting contamination by the fuel additive cerium oxide engineered nanoparticles within the United Kingdom and the associated risks," *Environmental Toxicology and Chemistry*, vol. 31, no. 11, pp. 2582–2587, 2012.

[9] U. Rajak, P. Nashine, P. K. Chaurasiya et al., "The effects on performance and emission characteristics of DI engine fuelled with CeO_2 nanoparticles addition in diesel/tyre pyrolysis oil blends," *Environment Development and Sustainability*, 2022.

[10] E. Kusmierek, "A CeO_2 semiconductor as a photocatalytic and photoelectrocatalytic material for the remediation of pollutants in industrial wastewater: a review," *Catalysts*, vol. 10, no. 12, Article ID 1435, 2020.

[11] V. Manikandan, R. Marnadu, J. Chandrasekaran et al., "Inherent characteristics of ultra-photosensitive Al/Cu-CeO_2/p-Si metal oxide semiconductor diodes," *Journal of Materials Chemistry C*, vol. 10, no. 4, pp. 1445–1457, 2022.

[12] A. García, L. Delgado, J. A. Torà et al., "Effect of cerium dioxide, titanium dioxide, silver, and gold nanoparticles on the activity of microbial communities intended in wastewater treatment," *Journal of Hazardous Materials*, vol. 199-200, pp. 64–72, 2012.

[13] A. Farfaletti, C. Astorga, G. Martini et al., "Effect of water/fuel emulsions and a cerium-based combustion improver additive on HD and LD diesel exhaust emissions," *Environmental Science & Technology*, vol. 39, no. 17, pp. 6792–6799, 2005.

[14] H. J. Jung, D. B. Kittelson, and M. R. Zachariah, "The influence of a cerium additive on ultrafine diesel particle emissions and kinetics of oxidation," *Combustion and Flame*, vol. 142, no. 3, pp. 276–288, 2005.

[15] B. Collin, M. Auffan, A. C. Johnson et al., "Environmental release, fate and ecotoxicological effects of manufactured ceria nanomaterials," *Environmental Science-Nano*, vol. 1, no. 6, pp. 533–548, 2014.

[16] A. Lazareva and A. A. Keller, "Estimating potential life cycle releases of engineered nanomaterials from wastewater treatment plants," *ACS Sustainable Chemistry & Engineering*, vol. 2, no. 7, pp. 1656–1665, 2014.

[17] S. Wagner, A. Gondikas, E. Neubauer, T. Hofmann, and F. von der Kammer, "Spot the difference: engineered and natural nanoparticles in the environment-release, behavior, and fate," *Angewandte Chemie-International Edition*, vol. 53, no. 46, pp. 12398–12419, 2014.

[18] K. Birbaum, R. Brogioli, M. Schellenberg et al., "No evidence for cerium dioxide nanoparticle translocation in maize plants," *Environmental Science & Technology*, vol. 44, no. 22, pp. 8718–8723, 2010.

[19] D. Cui, P. Zhang, Y. H. Ma et al., "Effect of cerium oxide nanoparticles on asparagus lettuce cultured in an agar medium," *Environmental Science-Nano*, vol. 1, no. 5, pp. 459–465, 2014.

[20] X. Gui, Z. Y. Zhang, S. T. Liu et al., "Fate and phytotoxicity of CeO_2 nanoparticles on lettuce cultured in the potting soil

environment," *PLOS ONE*, vol. 10, no. 8, Article ID e0134261, 2015.

[21] Y. Ma, L. Kuang, X. He et al., "Effects of rare earth oxide nanoparticles on root elongation of plants," *Chemosphere*, vol. 78, no. 3, pp. 273–279, 2010.

[22] S. Majumdar, J. R. Peralta-Videa, J. Trujillo-Reyes et al., "Soil organic matter influences cerium translocation and physiological processes in kidney bean plants exposed to cerium oxide nanoparticles," *Science of the Total Environment*, vol. 569-570, pp. 201–211, 2016.

[23] J. H. Priester, Y. Ge, R. E. Mielke et al., "Soybean susceptibility to manufactured nanomaterials with evidence for food quality and soil fertility interruption," *Proceedings of the National Academy of Sciences*, vol. 109, no. 37, pp. E2451–E2456, 2012.

[24] Q. Wang, X. Ma, W. Zhang, H. Pei, and Y. Chen, "The impact of cerium oxide nanoparticles on tomato (*Solanum lycopersicum* L.) and its implications for food safety," *Metallomics*, vol. 4, no. 10, pp. 1105–1112, 2012.

[25] P. Zhang, Y. H. Ma, S. T. Liu et al., "Phytotoxicity, uptake and transformation of nano-CeO_2 in sand cultured romaine lettuce," *Environmental Pollution*, vol. 220, Part B, pp. 1400–1408, 2017.

[26] P. Zhang, Y. H. Ma, Z. Y. Zhang et al., "Species-specific toxicity of ceria nanoparticles to *Lactuca* plants," *Nanotoxicology*, vol. 9, no. 1, pp. 1–8, 2015.

[27] J. R. Peralta-Videa, J. A. Hernandez-Viezcas, L. J. Zhao et al., "Cerium dioxide and zinc oxide nanoparticles alter the nutritional value of soil cultivated soybean plants," *Plant Physiology and Biochemistry*, vol. 80, pp. 128–135, 2014.

[28] E. Diatloff, F. W. Smith, and C. J. Asher, "Effects of lanthanum and cerium on the growth and mineral nutrition of corn and mungbean," *Annals of Botany*, vol. 101, no. 7, pp. 971–982, 2008.

[29] R. Shyam and N. C. Aery, "Effect of cerium on growth, dry matter production, biochemical constituents and enzymatic activities of cowpea plants [*Vigna unguiculata* (L.) Walp.]," *Journal of Soil Science and Plant Nutrition*, vol. 12, no. 1, pp. 1–14, 2012.

[30] D. Yuan, X.-Q. Shan, Q. Huai, B. Wen, and X. R. Zhu, "Uptake and distribution of rare earth elements in rice seeds cultured in fertilizer solution of rare earth elements," *Chemosphere*, vol. 43, no. 3, pp. 327–337, 2001.

[31] B. Li, Y. Chen, W.-Z. Liang et al., "Influence of cerium oxide nanoparticles on the soil enzyme activities in a soil-grass microcosm system," *Geoderma*, vol. 299, pp. 54–62, 2017.

[32] M. Auffan, D. Bertin, P. Chaurand et al., "Role of molting on the biodistribution of CeO_2 nanoparticles within *Daphnia pulex*," *Water Research*, vol. 47, no. 12, pp. 3921–3930, 2013.

[33] B. Collin, E. Oostveen, O. V. Tsyusko, and J. M. Unrine, "Influence of natural organic matter and surface charge on the toxicity and bioaccumulation of functionalized ceria nanoparticles in *Caenorhabditis elegans*," *Environmental Science & Technology*, vol. 48, no. 2, pp. 1280–1289, 2014.

[34] E. Lahive, K. Jurkschat, B. J. Shaw, R. D. Handy, D. J. Spurgeon, and C. Svendsen, "Toxicity of cerium oxide nanoparticles to the earthworm *Eisenia fetida*: subtle effects," *Environmental Chemistry*, vol. 11, no. 3, pp. 268–278, 2014.

[35] G. Cornelis, B. Ryan, M. J. McLaughlin, J. K. Kirby, D. Beak, and D. Chittleborough, "Solubility and batch retention of CeO_2 nanoparticles in soils," *Environmental Science & Technology*, vol. 45, no. 7, pp. 2777–2782, 2011.

[36] J. Fang, M.-H. Wang, D.-H. Lin, and B. Shen, "Enhanced transport of CeO_2 nanoparticles in porous media by macropores," *Science of the Total Environment*, vol. 543, Part 1, pp. 223–229, 2016.

[37] Z. Li, E. Sahle-Demessie, A. A. Hassan, and G. A. Sorial, "Transport and deposition of CeO_2 nanoparticles in water-saturated porous media," *Water Research*, vol. 45, no. 15, pp. 4409–4418, 2011.

[38] X. Lv, B. Gao, Y. Sun, X. Shi, H. Xu, and J. Wu, "Effects of humic acid and solution chemistry on the retention and transport of cerium dioxide nanoparticles in saturated porous media," *Water Air and Soil Pollution*, vol. 225, Article ID 2167, 2014.

[39] A. R. Petosa, C. Öhl, F. Rajput, and N. Tufenkji, "Mobility of nanosized cerium dioxide and polymeric capsules in quartz and loamy sands saturated with model and natural groundwaters," *Water Research*, vol. 47, no. 15, pp. 5889–5900, 2013.

[40] Z. Zhang, P. Gao, Y. Qiu, G. Liu, Y. Feng, and M. Wiesner, "Transport of cerium oxide nanoparticles in saturated silica media: influences of operational parameters and aqueous chemical conditions," *Scientific Reports*, vol. 6, Article ID 34135, 2016.

[41] A. A. Hassan, Z. Li, E. Sahle-Demessie, and G. A. Sorial, "Computational fluid dynamics simulation of transport and retention of nanoparticle in saturated sand filters," *Journal of Hazardous Materials*, vol. 244-245, pp. 251–258, 2013.

[42] M. C. Surette, J. A. Nason, S. L. Harper, and D. M. Mitrano, "What is "environmentally relevant"? A framework to advance research on the environmental fate and effects of engineered nanomaterials," *Environmental Science-Nano*, vol. 8, no. 9, pp. 2414–2429, 2021.

[43] J. R. Bathi, F. Moazeni, V. K. K. Upadhyayula et al., "Behavior of engineered nanoparticles in aquatic environmental samples: current status and challenges," *Science of the Total Environment*, vol. 793, Article ID 148560, 2021.

[44] O. Oriekhova and S. Stoll, "Stability of uncoated and fulvic acids coated manufactured CeO_2 nanoparticles in various conditions: from ultrapure to natural lake Geneva waters," *Science of the Total Environment*, vol. 562, pp. 327–334, 2016.

[45] O. Oriekhova and S. Stoll, "Effects of pH and fulvic acids concentration on the stability of fulvic acids–cerium (IV) oxide nanoparticle complexes," *Chemosphere*, vol. 144, pp. 131–137, 2016.

[46] M. Baalousha, "Effect of nanomaterial and media physicochemical properties on nanomaterial aggregation kinetics," *NanoImpact*, vol. 6, pp. 55–68, 2017.

[47] K. Li and Y. Chen, "Effect of natural organic matter on the aggregation kinetics of CeO_2 nanoparticles in KCl and $CaCl_2$ solutions: measurements and modeling," *Journal of Hazardous Materials*, vol. 209-210, pp. 264–270, 2012.

[48] B. Lv, C. Wang, J. Hou et al., "Influence of shear forces on the aggregation and sedimentation behavior of cerium dioxide (CeO_2) nanoparticles under different hydrochemical conditions," *Journal of Nanoparticle Research*, vol. 18, Article ID 193, 2016.

[49] K. Van Hoecke, K. A. C. De Schamphelaere, P. Van der Meeren, G. Smagghe, and C. R. Janssen, "Aggregation and ecotoxicity of CeO_2 nanoparticles in synthetic and natural waters with variable pH, organic matter concentration and ionic strength," *Environmental Pollution*, vol. 159, no. 4, pp. 970–976, 2011.

[50] G. X. You, J. Hou, Y. Xu, L. Z. Miao, Y. H. Ao, and B. S. Xing, "Surface properties and environmental transformations controlling the bioaccumulation and toxicity of cerium oxide nanoparticles: a critical review," in *Reviews of Environmental Contamination and Toxicology*, vol. 253 of *Reviews of Environmental Contamination and Toxicology*, pp. 155–206, Springer, Cham, 2021.

[51] S. Barany, K. Bohacs, I. Chepurna, and R. Meszaros, "Electrokinetic properties and stability of cerium dioxide suspensions," *RSC Advances*, vol. 6, no. 73, pp. 69343–69351, 2016.

[52] K. M. Buettner, C. I. Rinciog, and S. E. Mylon, "Aggregation kinetics of cerium oxide nanoparticles in monovalent and divalent electrolytes," *Colloids and Surfaces A: Physicochemical and Engineering Aspects*, vol. 366, no. 1–3, pp. 74–79, 2010.

[53] S. Bae, J. J. Lenhart, and Y. S. Hwang, "The effect of ionic strength, pH and natural organic matter on heteroaggregation of CeO_2 nanoparticles with montmorillonite clay minerals," *Environmental Engineering Research*, vol. 27, no. 6, Article ID 210470, 2022.

[54] F. Gómez-Rivera, J. A. Field, D. Brown, and R. Sierra-Alvarez, "Fate of cerium dioxide (CeO_2) nanoparticles in municipal wastewater during activated sludge treatment," *Bioresource Technology*, vol. 108, pp. 300–304, 2012.

[55] X. Liu, J. R. Ray, C. W. Neil, Q. Y. Li, and Y.-S. Jun, "Enhanced colloidal stability of CeO_2 nanoparticles by ferrous ions: adsorption, redox reaction, and surface precipitation," *Environmental Science & Technology*, vol. 49, no. 9, pp. 5476–5483, 2015.

[56] E. Tiwari, M. Mondal, N. Singh, N. Khandelwal, F. A. Monikh, and G. K. Darbha, "Effect of the irrigation water type and other environmental parameters on CeO_2 nanopesticide-clay colloid interactions," *Environmental Science-Processes & Impacts*, vol. 22, no. 1, pp. 84–94, 2020.

[57] X. Li, E. He, M. Zhang et al., "Interactions of CeO_2 nanoparticles with natural colloids and electrolytes impact their aggregation kinetics and colloidal stability," *Journal of Hazardous Materials*, vol. 386, Article ID 121973, 2020.

[58] B. Lv, C. Wang, J. Hou et al., "Towards a better understanding on aggregation behavior of CeO_2 nanoparticles in different natural waters under flow disturbance," *Journal of Hazardous Materials*, vol. 343, pp. 235–244, 2018.

[59] K. G. Li, W. Zhang, Y. Huang, and Y. S. Chen, "Aggregation kinetics of CeO_2 nanoparticles in KCl and $CaCl_2$ solutions: measurements and modeling," *Journal of Nanoparticle Research*, vol. 13, pp. 6483–6491, 2011.

[60] J. Song, Y. Xu, C. Liu et al., "Interpreting the role of NO_3^-, SO_4^{2-}, and extracellular polymeric substances on aggregation kinetics of CeO_2 nanoparticles: measurement and modeling," *Ecotoxicology and Environmental Safety*, vol. 194, Article ID 110456, 2020.

[61] B. Lv, C. Wang, J. Hou, P. Wang, L. Miao, and B. Xing, "Development of a comprehensive understanding of aggregation settling movement of CeO_2 nanoparticles in natural waters," *Environmental Pollution*, vol. 257, Article ID 113584, 2020.

[62] O. Oriekhova and S. Stoll, "Heteroaggregation of CeO_2 nanoparticles in presence of alginate and iron (III) oxide," *Science of the Total Environment*, vol. 648, pp. 1171–1178, 2019.

[63] J. T. K. Quik, I. Lynch, K. Van Hoecke et al., "Effect of natural organic matter on cerium dioxide nanoparticles settling in model fresh water," *Chemosphere*, vol. 81, no. 6, pp. 711–715, 2010.

[64] U. Dippon, S. Pabst, and S. Klitzke, "Colloidal stabilization of CeO_2 nanomaterials with polyacrylic acid, polyvinyl alcohol or natural organic matter," *Science of the Total Environment*, vol. 645, pp. 1153–1158, 2018.

[65] C. Li, A. Hassan, M. Palmai, P. T. Snee, P. C. Baveye, and C. J. G. Darnault, "Colloidal stability and aggregation kinetics of nanocrystal CdSe/ZnS quantum dots in aqueous systems: effects of pH and organic ligands," *Journal of Nanoparticle Research*, vol. 22, Article ID 349, 2020.

[66] Y. Xiao, W. Tang, W. J. G. M. Peijnenburg et al., "Aggregation, solubility and cadmium-adsorption capacity of CuO nanoparticles in aquatic environments: effects of pH, natural organic matter and component addition sequence," *Journal of Environmental Management*, vol. 310, Article ID 114770, 2022.

[67] I. G. Godinez and C. J. G. Darnault, "Aggregation and transport of nano-TiO_2 in saturated porous media: effects of pH, surfactants and flow velocity," *Water Research*, vol. 45, no. 2, pp. 839–851, 2011.

[68] S. Ghosh, H. Mashayekhi, B. Pan, P. Bhowmik, and B. S. Xing, "Colloidal behavior of aluminum oxide nanoparticles as affected by pH and natural organic matter," *Langmuir*, vol. 24, no. 21, pp. 12385–12391, 2008.

[69] B. J. R. Thio, D. Zhou, and A. A. Keller, "Influence of natural organic matter on the aggregation and deposition of titanium dioxide nanoparticles," *Journal of Hazardous Materials*, vol. 189, no. 1-2, pp. 556–563, 2011.

[70] C. Li, A. Hassan, M. Palmai, P. Snee, P. C. Baveye, and C. J. G. Darnault, "Colloidal stability and aggregation kinetics of nanocrystal CdSe/ZnS quantum dots in aqueous systems: effects of ionic strength, electrolyte type, and natural organic matter," *SN Applied Sciences*, vol. 4, Article ID 101, 2022.

[71] R. D. Avellán-Llaguno, X. Zhang, P. Zhao et al., "Differential aggregation of polystyrene and titanium dioxide nanoparticles under various salinity conditions and against multiple proteins types," *Environmental Science and Pollution Research*, vol. 29, pp. 74173–74184, 2022.

[72] B. Uyusur, C. J. G. Darnault, P. T. Snee, E. Koken, A. R. Jacobson, and R. R. Wells, "Coupled effects of solution chemistry and hydrodynamics on the mobility and transport of quantum dot nanomaterials in the vadose zone," *Journal of Contaminant Hydrology*, vol. 118, no. 3-4, pp. 184–198, 2010.

[73] A. R. Pales, E. N. Kinsey, C. Li et al., "Rheological properties of silica nanoparticles in brine and brine-surfactant systems," *Journal of Nanofluids*, vol. 6, no. 5, pp. 795–803, 2017.

[74] L. Bai, C. Li, C. Korte et al., "Effects of silica-based nanostructures with raspberry-like morphology and surfactant on the interfacial behavior of light, medium, and heavy crude oils at oil-aqueous interfaces," *Applied Nanoscience*, vol. 7, pp. 947–972, 2017.

[75] B. M. J. Huibers, A. R. Pales, L. Bai et al., "Wettability alteration of sandstones by silica nanoparticle dispersions in light and heavy crude oil," *Journal of Nanoparticle Research*, vol. 19, Article ID 323, 2017.

[76] H. Wang, X. Han, Y. Chen et al., "Effects of F^-, Cl^-, Br^-, NO_3^- and SO_4^{2-} on the colloidal stability of Fe_3O_4 nanoparticles in the aqueous phase," *Science of the Total Environment*, vol. 757, Article ID 143962, 2021.

[77] A. R. Petosa, D. P. Jaisi, I. R. Quevedo, M. Elimelech, and N. Tufenkji, "Aggregation and deposition of engineered

nanomaterials in aquatic environments: role of physicochemical interactions," *Environmental Science & Technology*, vol. 44, no. 17, pp. 6532–6549, 2010.

[78] I. G. Godinez, C. J. G. Darnault, A. P. Khodadoust, and D. Bogdan, "Deposition and release kinetics of nano-TiO_2 in saturated porous media: effects of solution ionic strength and surfactants," *Environmental Pollution*, vol. 174, pp. 106–113, 2013.

[79] R. A. French, A. R. Jacobson, B. Kim, S. L. Isley, R. L. Penn, and P. C. Baveye, "Influence of ionic strength, pH, and cation valence on aggregation kinetics of titanium dioxide nanoparticles," *Environmental Science & Technology*, vol. 43, no. 5, pp. 1354–1359, 2009.

[80] K. J. Wilkinson, E. Balnois, G. G. Leppard, and J. Buffle, "Characteristic features of the major components of freshwater colloidal organic matter revealed by transmission electron and atomic force microscopy," *Colloids and Surfaces A: Physicochemical and Engineering Aspects*, vol. 155, no. 2-3, pp. 287–310, 1999.

[81] F. H. Frimmel and G. Abbt-Braun, "Basic characterization of reference NOM from central Europe—similarities and differences," *Environment International*, vol. 25, no. 2-3, pp. 191–207, 1999.

[82] C. Chen and X. Wang, "Sorption of Th (IV) to silica as a function of pH, humic/fulvic acid, ionic strength, electrolyte type," *Applied Radiation and Isotopes*, vol. 65, no. 2, pp. 155–163, 2007.

[83] L. Liang, L. Luo, and S. Z. Zhang, "Adsorption and desorption of humic and fulvic acids on SiO_2 particles at nano- and micro-scales," *Colloids and Surfaces A: Physicochemical and Engineering Aspects*, vol. 384, no. 1–3, pp. 126–130, 2011.

[84] M. Baalousha, J. R. Lead, and Y. Ju-Nam, "Natural colloids and manufactured nanoparticles in aquatic and terrestrial systems," *Treatise on Water Science*, vol. 3, pp. 89–129, 2011.

[85] S. Ghosh, H. Mashayekhi, P. Bhowmik, and B. Xing, "Colloidal stability of Al_2O_3 nanoparticles as affected by coating of structurally different humic acids," *Langmuir*, vol. 26, no. 2, pp. 873–879, 2010.

[86] H. Hyung and J.-H. Kim, "Natural organic matter (NOM) adsorption to multi-walled carbon nanotubes: effect of NOM characteristics and water quality parameters," *Environmental Science & Technology*, vol. 42, no. 12, pp. 4416–4421, 2008.

[87] H. Mashayekhi, S. Ghosh, P. Du, and B. Xing, "Effect of natural organic matter on aggregation behavior of C_{60} fullerene in water," *Journal of Colloid and Interface Science*, vol. 374, no. 1, pp. 111–117, 2012.

[88] L. Mu and C. J. G. Darnault, "Colloidal phenomena and aggregation mechanisms of cerium oxide nanoparticles in aqueous systems: effects of monovalent and divalent cations, and Suwanee River humic and fulvic acids," *Journal of Nanoparticle Research*, vol. 25, Article ID 71, 2023.

[89] M. Baalousha, Y. Nur, I. Römer, M. Tejamaya, and J. R. Lead, "Effect of monovalent and divalent cations, anions and fulvic acid on aggregation of citrate-coated silver nanoparticles," *Science of the Total Environment*, vol. 454-455, pp. 119–131, 2013.

[90] K. L. Chen, S. E. Mylon, and M. Elimelech, "Aggregation kinetics of alginate-coated hematite nanoparticles in monovalent and divalent electrolytes," *Environmental Science & Technology*, vol. 40, no. 5, pp. 1516–1523, 2006.

[91] X. Li, J. J. Lenhart, and H. W. Walker, "Dissolution-accompanied aggregation kinetics of silver nanoparticles," *Langmuir*, vol. 26, no. 22, pp. 16690–16698, 2010.

[92] K. A. D. Guzman, M. P. Finnegan, and J. F. Banfield, "Influence of surface potential on aggregation and transport of titania nanoparticles," *Environmental Science & Technology*, vol. 40, no. 24, pp. 7688–7693, 2006.

[93] E. M. Hotze, T. Phenrat, and G. V. Lowry, "Nanoparticle aggregation: challenges to understanding transport and reactivity in the environment," *Journal of Environmental Quality*, vol. 39, no. 6, pp. 1909–1924, 2010.

[94] Y. Chen, Q. Gao, W. Chen et al., "A mechanistic study of stable dispersion of titanium oxide nanoparticles by humic acid," *Water Research*, vol. 135, pp. 85–94, 2018.

[95] D. Palomino, C. Yamunake, P. Le Coustumer, and S. Stoll, "Stability of TiO_2 nanoparticles in presence of fulvic acids. Importance of pH," *Journal of Colloid Science and Biotechnology*, vol. 2, no. 1, pp. 62–69, 2013.

[96] J. P. Jolivet, M. Henry, and J. Livage, *Metal Oxide Chemistry and Synthesis: From Solution to Solid*, Wiley, State, 2000.

[97] H. Wang, J. Qi, A. A. Keller, M. Zhu, and F. Li, "Effects of pH, ionic strength and humic acid on the removal of TiO_2 nanoparticles from aqueous phase by coagulation," *Colloids and Surfaces A: Physicochemical and Engineering Aspects*, vol. 450, pp. 161–165, 2014.

[98] M. Baalousha, A. Manciulea, S. Cumberland, K. Kendall, and J. R. Lead, "Aggregation and surface properties of iron oxide nanoparticles: influence of pH and natural organic matter," *Environmental Toxicology and Chemistry*, vol. 27, no. 9, pp. 1875–1882, 2008.

[99] Y. Yang, N. Nakada, R. Nakajima, M. Yasojima, C. Wang, and H. Tanaka, "pH, ionic strength and dissolved organic matter alter aggregation of fullerene C_{60} nanoparticles suspensions in wastewater," *Journal of Hazardous Materials*, vol. 244-245, pp. 582–587, 2013.

[100] W. Liu, W. L. Sun, A. G. L. Borthwick, and J. R. Ni, "Comparison on aggregation and sedimentation of titanium dioxide, titanate nanotubes and titanate nanotubes-TiO_2: influence of pH, ionic strength and natural organic matter," *Colloids and Surfaces A: Physicochemical and Engineering Aspects*, vol. 434, pp. 319–328, 2013.

[101] F. M. Omar, H. A. Aziz, and S. Stoll, "Aggregation and disaggregation of ZnO nanoparticles: influence of pH and adsorption of Suwannee River humic acid," *Science of the Total Environment*, vol. 468-469, pp. 195–201, 2014.

[102] S.-W. Bian, I. A. Mudunkotuwa, T. Rupasinghe, and V. H. Grassian, "Aggregation and dissolution of 4 nm ZnO nanoparticles in aqueous environments: influence of pH, ionic strength, size, and adsorption of humic acid," *Langmuir*, vol. 27, no. 10, pp. 6059–6068, 2011.

[103] M. Zhu, H. Wang, A. A. Keller, T. Wang, and F. Li, "The effect of humic acid on the aggregation of titanium dioxide nanoparticles under different pH and ionic strengths," *Science of the Total Environment*, vol. 487, pp. 375–380, 2014.

[104] M. Baalousha, "Aggregation and disaggregation of iron oxide nanoparticles: influence of particle concentration, pH and natural organic matter," *Science of the Total Environment*, vol. 407, no. 6, pp. 2093–2101, 2009.

[105] H. Wang, X. Zhao, X. Han et al., "Effects of monovalent and divalent metal cations on the aggregation and suspension of Fe_3O_4 magnetic nanoparticles in aqueous solution," *Science of the Total Environment*, vol. 586, pp. 817–826, 2017.

[106] I. Fernando and Y. Zhou, "Impact of pH on the stability, dissolution and aggregation kinetics of silver nanoparticles," *Chemosphere*, vol. 216, pp. 297–305, 2019.

[107] M. Delay, T. Dolt, A. Woellhaf, R. Sembritzki, and F. H. Frimmel, "Interactions and stability of silver nanoparticles in the aqueous phase: influence of natural organic matter (NOM) and ionic strength," *Journal of Chromatography A*, vol. 1218, no. 27, pp. 4206–4212, 2011.

[108] A. M. Vindedahl, J. H. Strehlau, W. A. Arnold, and R. L. Penn, "Organic matter and iron oxide nanoparticles: aggregation, interactions, and reactivity," *Environmental Science-Nano*, vol. 3, no. 3, pp. 494–505, 2016.

[109] F. Xu, "Review of analytical studies on TiO_2 nanoparticles and particle aggregation, coagulation, flocculation, sedimentation, stabilization," *Chemosphere*, vol. 212, pp. 662–677, 2018.

[110] M. Shen, X. Hai, Y. Shang et al., "Insights into aggregation and transport of graphene oxide in aqueous and saturated porous media: complex effects of cations with different molecular weight fractionated natural organic matter," *Science of the Total Environment*, vol. 656, pp. 843–851, 2019.

[111] F. Loosli, P. Le Coustumer, and S. Stoll, "TiO_2 nanoparticles aggregation and disaggregation in presence of alginate and Suwannee River humic acids. pH and concentration effects on nanoparticle stability," *Water Research*, vol. 47, no. 16, pp. 6052–6063, 2013.

[112] H. H. Wang, R. M. Burgess, M. G. Cantwell et al., "Stability and aggregation of silver and titanium dioxide nanoparticles in seawater: role of salinity and dissolved organic carbon," *Environmental Toxicology and Chemistry*, vol. 33, no. 5, pp. 1023–1029, 2014.

[113] L. Chekli, S. Phuntsho, M. Roy, and H. K. Shon, "Characterisation of Fe-oxide nanoparticles coated with humic acid and Suwannee River natural organic matter," *Science of the Total Environment*, vol. 461-462, pp. 19–27, 2013.

[114] M. Erhayem and M. Sohn, "Stability studies for titanium dioxide nanoparticles upon adsorption of Suwannee River humic and fulvic acids and natural organic matter," *Science of the Total Environment*, vol. 468-469, pp. 249–257, 2014.

[115] O. Furman, S. Usenko, and B. L. T. Lau, "Relative importance of the humic and fulvic fractions of natural organic matter in the aggregation and deposition of silver nanoparticles," *Environmental Science & Technology*, vol. 47, no. 3, pp. 1349–1356, 2013.

[116] X. Qu, Y. Hwang, P. J. J. Alvarez, D. Bouchard, and Q. Li, "UV irradiation and humic acid mediate aggregation of aqueous fullerene (nC_{60}) nanoparticles," *Environmental Science & Technology*, vol. 44, no. 20, pp. 7821–7826, 2010.

[117] N. Akaighe, S. W. Depner, S. Banerjee, and M. Sohn, "Transport and deposition of Suwannee River humic acid/natural organic matter formed silver nanoparticles on silica matrices: the influence of solution pH and ionic strength," *Chemosphere*, vol. 92, no. 4, pp. 406–412, 2013.

[118] C.-E. Hsiung, H.-L. Lien, A. E. Galliano, C.-S. Yeh, and Y.-H. Shih, "Effects of water chemistry on the destabilization and sedimentation of commercial TiO_2 nanoparticles: role of double-layer compression and charge neutralization," *Chemosphere*, vol. 151, pp. 145–151, 2016.

[119] Z. Wang, L. Zhang, J. Zhao, and B. Xing, "Environmental processes and toxicity of metallic nanoparticles in aquatic systems as affected by natural organic matter," *Environmental Science: Nano*, vol. 3, no. 2, pp. 240–255, 2016.

[120] J.-D. Hu, Y. Zevi, X.-M. Kou, J. Xiao, X.-J. Wang, and Y. Jin, "Effect of dissolved organic matter on the stability of magnetite nanoparticles under different pH and ionic strength conditions," *Science of the Total Environment*, vol. 408, no. 16, pp. 3477–3489, 2010.

[121] K. L. Chen and M. Elimelech, "Influence of humic acid on the aggregation kinetics of fullerene (C_{60}) nanoparticles in monovalent and divalent electrolyte solutions," *Journal of Colloid and Interface Science*, vol. 309, no. 1, pp. 126–134, 2007.

[122] K. A. Huynh and K. L. Chen, "Aggregation kinetics of citrate and polyvinylpyrrolidone coated silver nanoparticles in monovalent and divalent electrolyte solutions," *Environmental Science & Technology*, vol. 45, no. 13, pp. 5564–5571, 2011.

[123] N. Akaighe, S. W. Depner, S. Banerjee, V. K. Sharma, and M. Sohn, "The effects of monovalent and divalent cations on the stability of silver nanoparticles formed from direct reduction of silver ions by Suwannee River humic acid/natural organic matter," *Science of the Total Environment*, vol. 441, pp. 277–289, 2012.

[124] M. H. Shen, Y. G. Yin, A. Booth, and J. F. Liu, "Effects of molecular weight-dependent physicochemical heterogeneity of natural organic matter on the aggregation of fullerene nanoparticles in mono- and di-valent electrolyte solutions," *Water Research*, vol. 71, pp. 11–20, 2015.

[125] J. F. Liu, S. Legros, F. Von der Kammer, and T. Hofmann, "Natural organic matter concentration and hydrochemistry influence aggregation kinetics of functionalized engineered nanoparticles," *Environmental Science & Technology*, vol. 47, no. 9, pp. 4113–4120, 2013.

[126] L. Chekli, S. Phuntsho, L. D. Tijing, J. L. Zhou, J. H. Kim, and H. K. Shon, "Stability of Fe-oxide nanoparticles coated with natural organic matter under relevant environmental conditions," *Water Science and Technology*, vol. 70, no. 12, pp. 2040–2046, 2014.

[127] Y. Zhang, Y. S. Chen, P. Westerhoff, and J. Crittenden, "Impact of natural organic matter and divalent cations on the stability of aqueous nanoparticles," *Water Research*, vol. 43, no. 17, pp. 4249–4257, 2009.

[128] X. Liu, M. Wazne, T. Chou, R. Xiao, and S. Xu, "Influence of Ca^{2+} and Suwannee River humic acid on aggregation of silicon nanoparticles in aqueous media," *Water Research*, vol. 45, no. 1, pp. 105–112, 2011.

[129] R. F. Domingos, N. Tufenkji, and K. J. Wilkinson, "Aggregation of titanium dioxide nanoparticles: role of a fulvic acid," *Environmental Science & Technology*, vol. 43, no. 5, pp. 1282–1286, 2009.

[130] W. Zhang, U.-S. Rattanaudompol, H. Li, and D. Bouchard, "Effects of humic and fulvic acids on aggregation of aqu/nC_{60} nanoparticles," *Water Research*, vol. 47, no. 5, pp. 1793–1802, 2013.

[131] M. Baalousha, M. Motelica-Heino, and P. Le Coustumer, "Conformation and size of humic substances: effects of major cation concentration and type, pH, salinity, and residence time," *Colloids and Surfaces A: Physicochemical and Engineering Aspects*, vol. 272, no. 1-2, pp. 48–55, 2006.

[132] J. D. Ritchie and E. M. Perdue, "Proton-binding study of standard and reference fulvic acids, humic acids, and natural organic matter," *Geochimica et Cosmochimica Acta*, vol. 67, no. 1, pp. 85–96, 2003.

[133] I. L. Gunsolus, M. P. S. Mousavi, K. Hussein, P. Buhlmann, and C. L. Haynes, "Effects of humic and fulvic acids on silver nanoparticle stability, dissolution, and toxicity," *Environmental Science & Technology*, vol. 49, no. 13, pp. 8078–8086, 2015.

[134] S. D. Saab, E. R. Carvalho, R. Bernardes, M. R. de Moura, L. Martin-Neto, and L. H. C. Mattoso, "pH effect in aquatic fulvic acid from a Brazilian river," *Journal of the Brazilian Chemical Society*, vol. 21, no. 8, pp. 1490–1496, 2010.

[135] G. Sposito, *The Chemistry of Soils*, Oxford University Press, 2nd edition, 2008.

[136] L. Mu, *Stability and Toxicity of Cerium Oxide Nanoparticles in Water-Soil-Plant Systems*, Clemson University, Clemson, SC, United States, 2019.